trappc11 is required for protein glycosylation in zebrafish and humans

Charles DeRossi[a,b,†], Ana Vacaru[a,b,†], Ruhina Rafiq[a,b], Ayca Cinaroglu[a,b], Dru Imrie[a,c], Shikha Nayar[d], Anastasia Baryshnikova[e], Miroslav P. Milev[f], Daniela Stanga[f], Dhara Kadakia[a], Ningguo Gao[g], Jaime Chu[d], Hudson H. Freeze[h], Mark A. Lehrman[g], Michael Sacher[f,i], and Kirsten C. Sadler[a,b,c,‡,*]

[a]Department of Medicine, Division of Liver Diseases, [b]Department of Developmental and Regenerative Biology, [c]Graduate School of Biomedical Sciences, and [d]Department of Pediatrics and Mindich Institute for Child Health, Icahn School of Medicine at Mount Sinai, New York, NY 10029; [e]Lewis-Sigler Institute for Integrative Genomics, Princeton University, Princeton, NJ 08544; [f]Department of Biology, Concordia University, Montreal, QC H4B 1R6, Canada; [g]Department of Pharmacology, University of Texas Southwestern Medical Center, Dallas, TX 75390; [h]Sanford Children's Health Research Center, Sanford Burnham Prebys Medical Discovery Institute, La Jolla, CA 92037; [i]Department of Anatomy and Cell Biology, McGill University, Montreal, QC H3A 0C7, Canada

ABSTRACT **Activation of the unfolded protein response (UPR) can be either adaptive or pathological. We term the pathological UPR that causes fatty liver disease a "stressed UPR." Here we investigate the mechanism of stressed UPR activation in zebrafish bearing a mutation in the *trappc11* gene, which encodes a component of the transport protein particle (TRAPP) complex. *trappc11* mutants are characterized by secretory pathway defects, reflecting disruption of the TRAPP complex. In addition, we uncover a defect in protein glycosylation in *trappc11* mutants that is associated with reduced levels of lipid-linked oligosaccharides (LLOs) and compensatory up-regulation of genes in the terpenoid biosynthetic pathway that produces the LLO anchor dolichol. Treating wild-type larvae with terpenoid or LLO synthesis inhibitors phenocopies the stressed UPR seen in *trappc11* mutants and is synthetically lethal with *trappc11* mutation. We propose that reduced LLO level causing hypoglycosylation is a mechanism of stressed UPR induction in *trappc11* mutants. Of importance, in human cells, depletion of TRAPPC11, but not other TRAPP components, causes protein hypoglycosylation, and lipid droplets accumulate in fibroblasts from patients with the *TRAPPC11* mutation. These data point to a previously unanticipated and conserved role for TRAPPC11 in LLO biosynthesis and protein glycosylation in addition to its established function in vesicle trafficking.**

Monitoring Editor
Reid Gilmore
University of Massachusetts

Received: Aug 10, 2015
Revised: Feb 12, 2016
Accepted: Feb 19, 2016

This article was published online ahead of print in MBoC in Press (http://www.molbiolcell.org/cgi/doi/10.1091/mbc.E15-08-0557) on February 24, 2016.

†These authors contributed equally.

‡Present address: Biology Program, New York University Abu Dhabi, Box 12988 Saadiyat Campus, Abu Dhabi, United Arab Emirates.

*Address correspondence to: Kirsten C. Sadler (kirsten.edepli@nyu.edu).

Abbreviations used: Atv, atorvastatin; BFA, brefeldin A; Endo H, endoglycosidase H; Gc-EGFP, group component–enhanced green fluorescent protein; LLO, lipid-linked oligosaccharide; PC1, first principal component; PNGase F, peptide-*N*-glycosidase F; Tm, tunicamycin; TRAPα, translocon-associated protein subunit α; TRAPP, transport protein particle; UPR, unfolded protein response.

INTRODUCTION

Fatty liver disease impairs protein secretion from hepatocytes and contributes to its associated morbidity and mortality. Endoplasmic reticulum (ER) dysfunction, frequently referred to as ER stress, is central to metabolic diseases, including fatty liver disease (Imrie and Sadler, 2012; Wang and Kaufman, 2014). Several questions concerning how the protein secretory pathway intersects with the metabolic pathway remain unanswered. In particular, it is unknown what kinds of cellular stresses can induce a disease-promoting unfolded protein response (UPR).

The ER is the site of protein folding, glycosylation, quality control, packaging, and export of correctly folded and adequately glycosylated proteins bound for the cell membrane and extracellular space. Insufficiency in any of these processes results in accumulation of unfolded or misfolded proteins in the ER, causing activation of

Supplemental Material can be found at:
http://www.molbiolcell.org/content/suppl/2016/02/22/mbc.E15-08-0557v1.DC1.html

the UPR to correct this burden. The UPR increases expression of proteins that promote degradation of misfolded secretory cargo and enhances the protein folding capacity of the ER. In addition, UPR activation inhibits translation of new proteins until the unfolded protein backlog can be ameliorated or the cell can adapt.

Persistent unfolded protein accumulation producing chronic UPR activation is termed ER stress, and this pathological state is associated with cell dysfunction and death. Whereas some types of insults cause ER stress, others induce an adaptive UPR that is permissive to cell function and survival. Considering the dual nature of the UPR, it is of interest to identify which types of cell stressors cause a useful, adaptive UPR and which induce a pathological UPR. The terminology used to discuss the UPR needs to be refined, as the term ER stress is too broad for studies focused on specific stress responses that have distinct outcomes. To provide a lexicon to facilitate studies that differentiate between UPRs, we previously defined a distinct UPR subclass that was significantly correlated with steatosis in zebrafish and human liver samples (Vacaru *et al.*, 2014a). We termed this subclass a "stressed UPR" to differentiate it from other types of UPR, such as the adaptive (Rutkowski and Kaufman, 2007) and terminal (Oakes and Papa, 2015) UPRs, which have different gene expression profiles and, of importance, very different outcomes. Most significantly, we showed that a stressed UPR is pathogenic for fatty liver disease (Vacaru *et al.*, 2014a). Here we sought to identify cellular stresses that could induce a stressed UPR and cause fatty liver.

foie gras (*foigr*) mutant zebrafish develop lipid accumulation in hepatocytes (steatosis; Sadler *et al.*, 2005) associated with high activation of many UPR target genes (Cinaroglu *et al.*, 2011). UPR activation is essential for steatosis in *foigr* mutants and in other cases of fatty liver, as blocking activating transcription factor 6 (Atf6), a main UPR effector, reduced fatty liver caused by *foigr* mutation, tunicamycin (Tm) treatment (Cinaroglu *et al.*, 2011), and alcohol exposure (Howarth *et al.*, 2014). Because overexpression of Atf6 in hepatocytes causes fatty liver in the absence of stress (Howarth *et al.*, 2014), we concluded that the UPR is both necessary and sufficient for steatosis and that Atf6 is a primary mediator of UPR-induced fatty liver. The aim of this study was to understand the nature of the stress that can induce this unique, disease-causing, stressed UPR.

foigr mutants contain a viral DNA insertion in a gene encoding the zebrafish homologue of transport protein particle (TRAPP) 11 (TRAPPC11; Amsterdam *et al.*, 2004; Sadler *et al.*, 2005). The TRAPP complex tethers ER-derived vesicles to the *cis*-Golgi and functions as a GTP exchange factor for Rab1a, which ultimately recruits soluble *N*-ethylmaleimide–sensitive factor attachment protein receptor proteins to mediate vesicle fusion with target membranes (Barrowman *et al.*, 2010). Some TRAPP members, including TRAPPC3 and TRAPPC11, are critical for TRAPP complex integrity and stability in mammalian cells, as depletion of these proteins results in disruption of the complex followed by fragmentation of the Golgi apparatus and the ER-to-Golgi intermediate compartment (Scrivens *et al.*, 2011). Patients with a mutation in *TRAPPC11* have recently been described, and, strikingly, one such patient presented with steatosis (Liang *et al.*, 2015). Thus fatty liver is a conserved response to mutation of *TRAPPC11*.

Most components of the TRAPP complex are highly conserved from yeast to humans. However, a few components, such as TrappC11, 12, and 13, are absent from yeast (Scrivens *et al.*, 2011), although they are conserved throughout metazoans and are found in some plant species. The implications of this are not well understood, but one possibility is that multicellular organisms may have evolved novel TRAPP components that have the flexibility to take on functions outside of the TRAPP complex. The differences in the clinical presentation of patients with mutations in different TRAPP complex members may also point to unique or tissue-specific roles for these different proteins. For example, *TRAPPC11* patients present with limb girdle muscular dystrophy type 2S and intellectual disability (Bogershausen *et al.*, 2013), whereas patients with *TRAPPC2* mutations develop spondyloepiphyseal dysplasia tarda, a disease characterized by skeletal malformations (Gedeon *et al.*, 1999). Furthermore, a recent report described a requirement for TRAPPC12 (also called TRAMM) in chromosome congression during mitosis, which is entirely separate from its capacity as a TRAPP complex member (Milev *et al.*, 2015). The ability to function in multiple cellular roles is not a unique feature of TRAPP complex proteins and has been observed in many cases in which mutations in proteins that are assumed to function in a fundamental cellular process cause discrete clinical syndromes (Vacaru *et al.*, 2014b).

Here we report that cells in the liver of zebrafish *trappc11* mutants display the expected defect in protein secretion that we attribute to disruption of the canonical function of the TRAPP complex. However, introducing a severe block in trafficking alone appeared to neither activate a stressed UPR in the liver nor cause steatosis. This suggested that disruption of some other pathway in *trappc11* mutants accounted for its phenotype. Biochemical, genetic, and pharmacological approaches point to a defect in terpenoid synthesis in *trappc11* mutants that leads to reduced N-linked protein glycosylation, subsequent activation of a stressed UPR, and steatosis. Of great importance, we found that human cells depleted of TRAPPC11, but not other TRAPP complex factors, have a marked loss of protein glycosylation. Furthermore, cells from patients with a *TRAPPC11* mutation show an increase in lipid accumulation, which is a prominent feature of *trappc11*-mutant hepatocytes in zebrafish. Thus we conclude that protein hypoglycosylation is a primary mechanism that induces a stressed UPR leading to fatty liver in *trappc11* mutants. Our data suggest that a glycosylation defect may underlie the pathophysiology of patients with *TRAPPC11* mutations.

RESULTS

trappc11 mutation causes a stressed UPR in the liver

foigr mutants contain a viral DNA insertion between exons 12 and 13 of the *trappc11* gene. As previously described (Sadler *et al.*, 2005), this insertion results in splicing of a portion of the viral DNA between these two exons, altering the protein-coding sequence so that the mutant allele contains the first 429 amino acids of the Trappc11 protein followed by 58 amino acids encoded by the viral DNA and a frameshift that introduces a premature stop codon. The predicted mutant protein product has an approximate molecular weight of 56 kDa (Sadler *et al.*, 2005). Western analysis of *trappc11* mutants, phenotypically wild-type (WT) siblings, and unrelated WT controls showed that mutants were devoid of the full-length Trappc11 protein (molecular weight 129 kDa) that is detected in WT and siblings. Instead, *trappc11* mutants showed enrichment of a 56-kDa immunoreactive protein, which we assume is the predicted truncated protein generated from the splice trap (Supplemental Figure S1). Mendelian ratios predict that two-thirds of the trappc11 siblings are *trappc11*$^{+/-}$, and we previously showed that they do express the mutant transcript (Sadler *et al.*, 2005). Here we show that they also express the predicted truncated protein but at lower levels than homozygous *trappc11* mutants. However, because *trappc11*$^{+/-}$ larvae do not have any features found in *trappc11*$^{-/-}$ mutants, we conclude that this mutation is not acting as a dominant negative.

We previously defined a distinct UPR, which we termed a stressed UPR, characterized by high expression of a panel of eight UPR effectors and target genes (Vacaru *et al.*, 2014a). A stressed

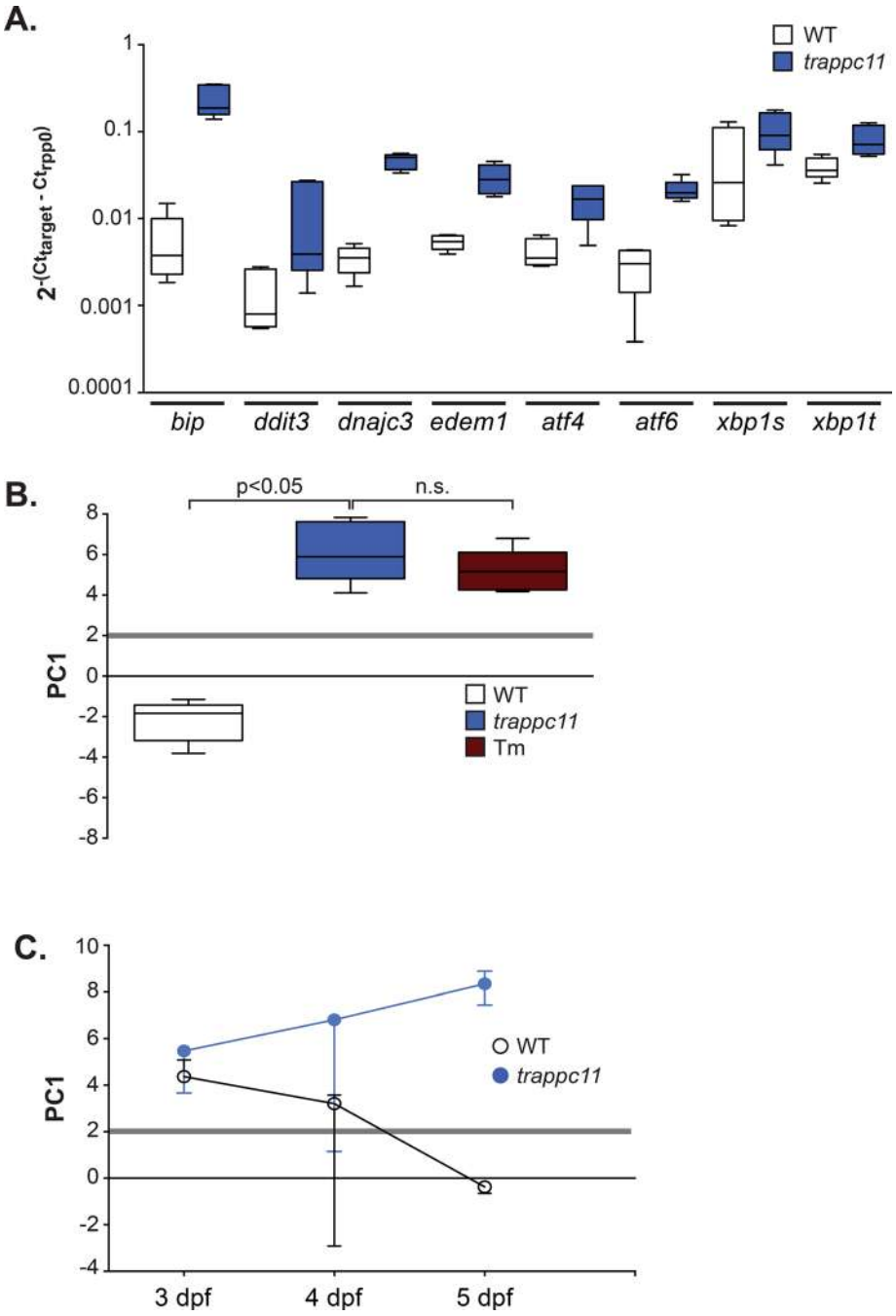

FIGURE 1: Mutation of *trappc11* in zebrafish causes a stressed UPR in the liver. (A) Livers from 5-dpf WT and *trappc11*-mutant zebrafish larvae were collected and analyzed by qPCR for expression of eight UPR effectors and target genes. *dCt* values normalized to the housekeeping gene *rpp0* are shown from five clutches. All genes are significantly increased, with $p < 0.05$ using a Student's paired *t* test. (B) The first principal component (PC1) of the eight UPR gene panel in A reveals that *trappc11* mutants, but not WT siblings, have a stressed UPR similar to that seen in Tm-treated larvae, indicated by a PC1 value >2 (gray line). n.s., not significant. (C) PC1 analysis of three clutches of WT and *trappc11* mutants during development shows that the UPR decreases over time in WT livers but remains elevated in *trappc11*-mutant livers at 4 and 5 dpf. Median PC1 values, with error bars indicating range. A stressed UPR with a PC1 value >2 is observed at all time points in mutant livers.

UPR was the only subclass that caused fatty liver disease in zebrafish and was also associated with fatty liver in humans (Vacaru *et al.*, 2014a). We hypothesized that fatty liver in the *trappc11* model was attributed to a stressed UPR and addressed this by quantitative PCR (qPCR) analysis of the expression of the eight-gene panel in livers dissected from 5-d postfertilization (dpf) *trappc11* mutants and their phenotypically WT siblings. All genes were significantly up-regulated in mutants (Figure 1A). We previously described the application of principal component (PC) analysis to the expression profile of this panel of genes in livers of zebrafish larvae exposed to three different stressors that act via different mechanisms: Tm, brefeldin A (BFA), and thapsigargin (Tg). We identified the first principal component (PC1), which captured >70% of the variability of the UPR target gene expression in these samples (Vacaru *et al.*, 2014a), and found that PC1 values >2.0 captured a stressed UPR and that this significantly correlated with steatosis incidence.

In this study, we found that the median PC1 in WT livers was –2, consistent with previous findings (Vacaru *et al.*, 2014a), and PC1 in *trappc11* mutant livers was nearly 6 (Figure 1B). This value was not significantly different from that in livers collected from WT larvae treated with 1 µg/ml Tm (Figure 1B and Supplemental Figure S2), a classical ER stress–inducing agent that we previously demonstrated to potently induce a stressed UPR (Cinaroglu *et al.*, 2011; Vacaru *et al.*, 2014a), which establishes that *trappc11* mutants have a stressed UPR.

The morphological phenotypes that characterize *trappc11*-mutant larvae develop after maternal *trappc11* mRNA has been depleted (Supplemental Figure S3A; Sadler *et al.*, 2005; Cinaroglu *et al.*, 2011). UPR genes were expressed at similar levels in WT and mutant livers at 3 dpf (Figure 1C and Supplemental Figure S3B). Of interest, at this stage of development, PC1 was >2.0 in both WT and *trappc11* mutants, reflecting the demand imposed by differentiation of highly secretory hepatocytes. However, at 4 and 5 dpf, as the liver matured, UPR gene expression (PC1) decreased in WT livers but remained elevated in *trappc11*-mutant livers (Figure 1C and Supplemental Figure S3B). We hypothesize that the persistence of the stressed UPR in *trappc11* mutants is a primary cause of steatosis in this model.

trappc11-mutant hepatocytes develop Golgi complex fragmentation and secretory cargo retention

Mammalian TRAPPC11 is a component of the vertebrate TRAPP complex (Scrivens *et al.*, 2011; Bassik *et al.*, 2013), and knockdown of the mammalian or insect homologues of *trappc11* in tissue culture cells results in Golgi apparatus fragmentation and inhibits protein secretion (Wendler *et al.*, 2010; Scrivens *et al.*, 2011; Bogershausen *et al.*, 2013). We hypothesized that the *trappc11*-mutant

phenotype would also be associated with a similar cellular phenotype, and perhaps the resulting secretory cargo backload could account for the stressed UPR in *trappc11*-mutant livers. To test this, we examined the structure of the Golgi apparatus in hepatocytes of 4- and 5-dpf *trappc11* mutants using transgenic zebrafish that express an enhanced green fluorescent protein (EGFP)–tagged *trans*-Golgi network marker, *Tg(actb2:GalT-EGFP)* (Gerhart *et al.*, 2012). In WT larvae, the Golgi apparatus appeared in the classical stacked ribbon configuration in nearly 90% of hepatocytes at both time points (Figure 2, A and B). In contrast, *trappc11* mutants developed fragmented and vesiculated Golgi in >70 and 90% of hepatocytes at 4 and 5 dpf, respectively (Figure 2, A and B). Thus, as expected, *trappc11* is required for maintaining the organization of the Golgi apparatus in zebrafish.

Ultrastructural analysis of hepatocytes from 5-dpf *trappc11* mutants revealed profound defects in ER morphology (Cinaroglu *et al.*, 2011). To further examine this across multiple larvae, we crossed transgenic zebrafish that localize td-Tomato to the ER in hepatocytes (*Tg(fabp10:ER-td-tomato)*) with *Tg(actb2:GalT-EGFP)* zebrafish to investigate the morphology of both organelles in the same cells. The fine reticular pattern of the ER found in most control hepatocytes (Figure 2, A and B) was distorted in *trappc11*-mutant hepatocytes, which had distended and vesiculated ER morphologies (asterisks in Figure 2A). Abnormal ER morphology was found in 31% of hepatocytes analyzed at 4 dpf (437 cells analyzed from 14 samples) and was significantly higher at 5 dpf, seen in 75% of hepatocytes ($p < 0.001$; 342 cells analyzed from eight samples; Figure 2B). Thus *trappc11* mutation causes major structural defects in secretory organelles in hepatocytes coincident with the onset of the gross morphological phenotype (Supplemental Figure S3A) and UPR activation (Figure 1C and Supplemental Figure S3B).

Previous studies in mammalian and insect cells demonstrated that loss of TRAPPC11 inhibits protein secretion (Wendler *et al.*, 2010; Scrivens *et al.*, 2011; Bogershausen *et al.*, 2013). We determined whether *trappc11* mutants also have a block in protein secretion by using a transgenic zebrafish line that expresses a GFP-tagged glycoprotein (group complement [Gc], which was also previously called vitamin D–binding protein) under a hepatocyte-specific promoter (*Tg(fabp10:Gc-EGFP)* (Xie *et al.*, 2010; Howarth *et al.*, 2013). Gc-EGFP was first detected in the liver of WT larvae at 3 dpf (arrows in Figure 2C, above the autofluorescent yolk) and became more abundant in the vasculature of older larvae due to secretion of this protein into the serum (Figure 2C, arrowheads). However, in *trappc11* mutants, despite their being morphologically normal at this stage (Supplemental Figure S3A), retention of the Gc-EGFP glycoprotein was detected in hepatocytes at 3 dpf. Retention became more pronounced as the fish aged (Figure 2C). This secretory defect was similar to that caused by treating WT larvae from 3 to 5 dpf with 1 µg/ml BFA, a known inhibitor of ER-to-Golgi glycoprotein transport (Figure 2C), which we previously showed causes dramatic fragmentation of the Golgi complex in zebrafish (Gerhart *et al.*, 2012; Vacaru *et al.*, 2014a). Consistent with ER retention, Gc-EGFP in *trappc11* mutants overlapped with a marker of the ER in *Tg(fabp10:ER-tdTomato)* but not in WT hepatocytes (Figure 2D).

The block in hepatocyte protein secretion was further examined by immunoblotting for Gc-EGFP in dissected livers and liverless carcasses from *trappc11* mutants and WT siblings at 5 dpf. Gc-EGFP protein was difficult to detect in WT liver samples, since nearly all of it was secreted and found in the carcass. In contrast, a striking abundance of Gc-EGFP was found in *trappc11*-mutant livers (Figure 2E), confirming a defect in its secretion. These results are consistent with Golgi abnormalities observed after *TrappC11* knockdown in human (Scrivens *et al.*, 2011) and insect (Wendler *et al.*, 2010) cells and in patient fibroblasts bearing mutations in *TRAPPC11* (Bogershausen *et al.*, 2013). Thus *trappc11* mutation in zebrafish causes Golgi apparatus fragmentation and blocks protein secretion from hepatocytes, consistent with a role in the canonical function of the TRAPP complex.

Despite confirming that *trappc11* mutation in zebrafish results in secretory pathway defects, we do not consider this to be the primary etiology of the stressed UPR leading to fatty liver phenotype, since we previously found that complete fragmentation of the Golgi complex in zebrafish hepatocytes after BFA treatment induced neither a stressed UPR nor fatty liver (Vacaru *et al.*, 2014a). Thus we conclude that blocking secretory cargo traffic via disruption of the TRAPP complex is not sufficient to induce the same type of UPR as occurs in *trappc11* mutants.

trappc11 mutation is phenocopied by Tm

Although BFA treatment failed to recapitulate the *trappc11*-mutant phenotype, we previously showed that Tm-treated larvae are strikingly similar in morphology (Figure 3A; Cinaroglu *et al.*, 2011), gene expression (Figure 1, A and B, and Supplemental Figure S2), and fatty liver incidence (Cinaroglu *et al.*, 2011). Tm blocks N-linked glycosylation by inhibiting DPAGT1, an enzyme that catalyzes the first step in lipid-linked oligosaccharide (LLO) synthesis, producing *N*-acetylglucosamine-diphosphodolichol (GlcNAc-PP-dol) from dolichol phosphate and UDP-GlcNAc (Lehrman *et al.*, 1988). Reduced LLO leads to insufficient glycan transfer to proteins (hypoglycosylation), resulting in protein misfolding and UPR induction.

On the basis of the phenotypic similarities, we asked whether *trappc11* mutants and Tm affected the same pathway. If so, treatment of *trappc11* mutants with Tm should result in either a synergistic effect or no effect on phenotype if either perturbation maximally affects a shared pathway. We tested this by exposing *trappc11* mutants to Tm concentrations ranging from 0.125 to 3 µg/ml from 3 to 5 dpf, which we previously identified as sufficient to induce a stressed UPR at the lower end and to be lethal at the higher end (Vacaru *et al.*, 2014a). Whereas the morphological phenotype of *trappc11* mutants was not altered by lower concentrations of Tm (Figure 3A), almost 20% of *trappc11* mutants exposed to 1 µg/ml Tm died by 5 dpf. A concentration of 3 µg/ml Tm was completely lethal to *trappc11* mutants, but >40% of their WT siblings survived this treatment (Figure 3, B and C). This indicates that *trappc11* is synthetically lethal with Tm. Furthermore, cotreatment of WT larvae with both Tm and BFA (Figure 3, B and C) also leads to increased lethality (likely due to acute compound drug exposure) but was not as severe as the synthetic lethality seen with Tm treatment of *trappc11* mutants, again suggesting that the latter is due to a synthetic lethality.

Despite the synthetic lethality of Tm treatment with *trappc11* mutation, Tm did not further activate the stressed UPR in *trappc11* mutants, as there was no additional increase of PC1 in the livers of *trappc11* mutants treated with 0.125 µg/ml Tm, a dose that produced intermediate UPR activation in control larvae (Figure 3D; Vacaru *et al.*, 2014a). These results suggest that the stressed UPR in *trappc11* mutants is maximally activated and that Tm, functioning in the same pathway, cannot further increase PC1. This conclusion is supported by the ability of treating *trappc11* larvae with 0.25 and 0.5 µM Tg, which causes ER stress by depleting ER calcium stores and so is in a pathway different from that of Tm, to dose dependently increase PC1 in *trappc11* mutants (Figure 3E). Thus the inability of Tm exposure to increase PC1 in *trappc11* mutants cannot be attributed to the system having reached a maximal level of induction. Instead,

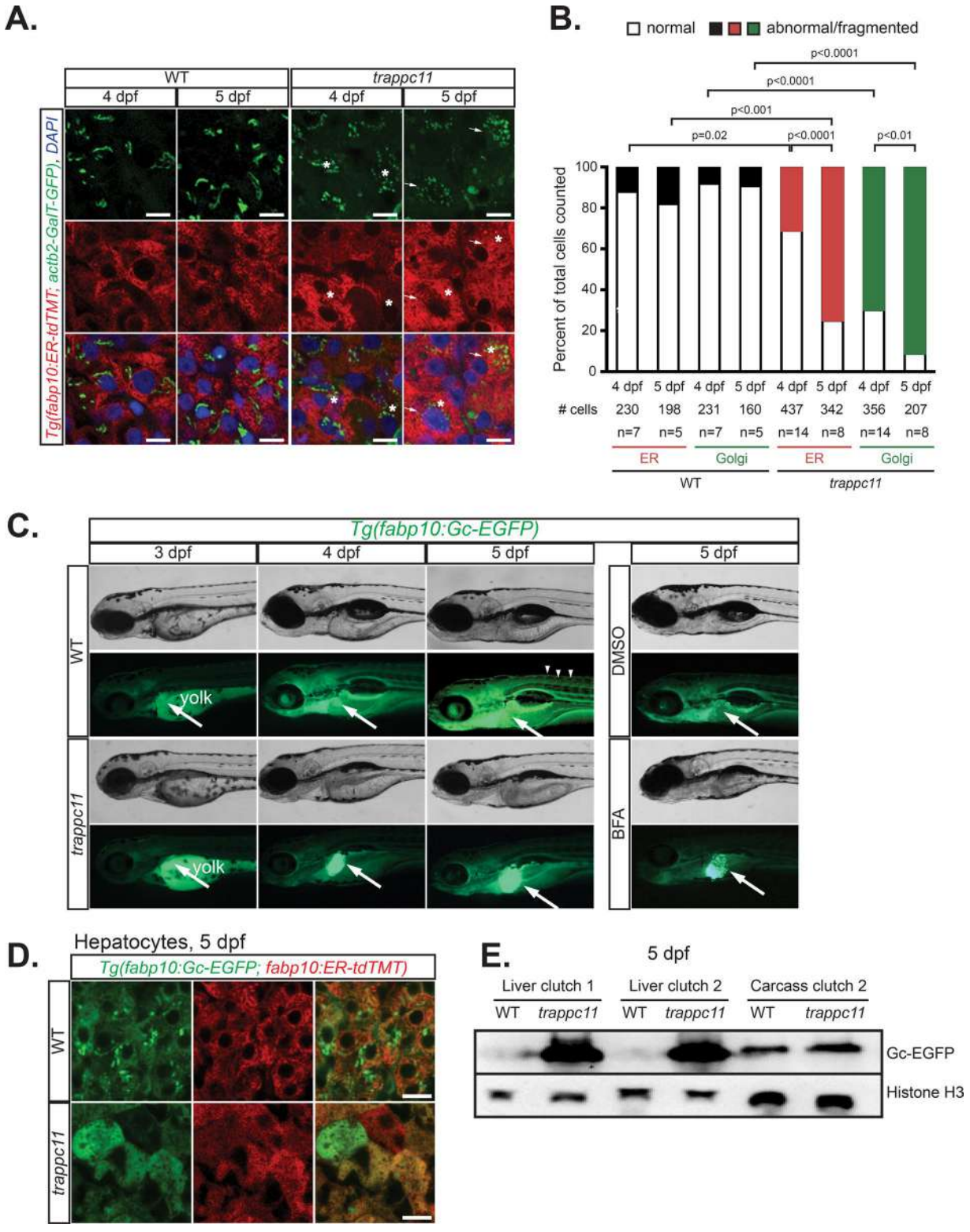

FIGURE 2: Mutation of *trappc11* in zebrafish causes secretory pathway defects. (A) Confocal microscopy on cryosections from 4- and 5-dpf *trappc11* mutants and phenotypically WT siblings that ubiquitously express a Golgi apparatus marker (green), *Tg(actb2:GalT-GFP)*, and a hepatocyte-specific ER marker (red), *Tg(fabp10:ER-td-TMT)*. Hepatocytes that show abnormal morphology, that is, fragmented Golgi apparatus and distended ER, are marked with arrows and asterisks, respectively, and quantified (B) as percentage abnormal to total hepatocytes counted (# cells) from number of fish counted (*n*). The *p* values were calculated using Fisher's exact test. (C) Bright-field and fluorescence images of 3- to 5-dpf WT and *trappc11* transgenic *Tg(fabp10:Gc-EGFP)* larvae demonstrate GFP accumulation in the liver of *trappc11* mutants, similar to that seen with BFA-treated (1 μg/ml) control larvae, which indicates defective protein secretion. Arrows indicate livers where Gc-EGFP is being produced, and arrowheads show secreted Gc-EGFP in

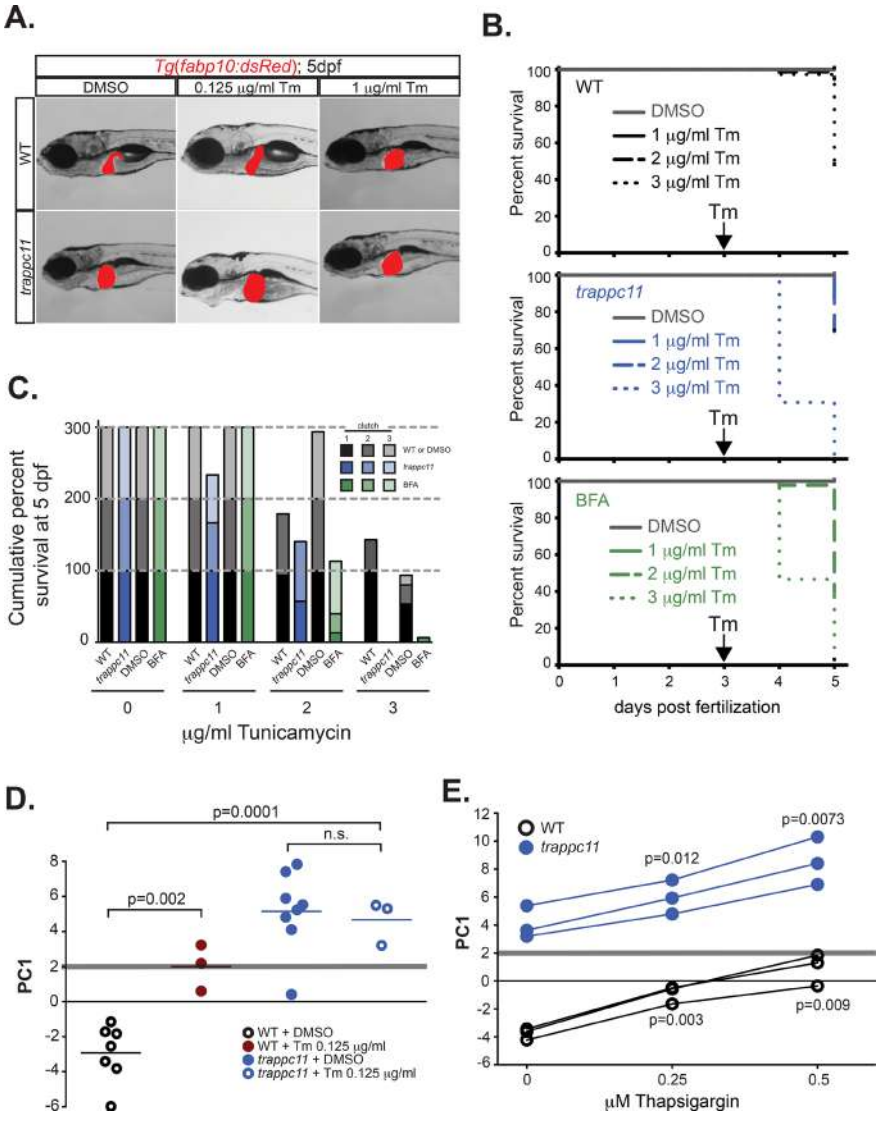

FIGURE 3: Tm phenocopies *trappc11* mutants and synergizes with *trappc11* mutation. (A) Transgenic WT and *trappc11* mutant larvae that express a hepatocyte-specific marker (*Tg(fabp10:dsRed)*) were exposed to sublethal doses of Tm at 3 dpf and analyzed at 5 dpf for gross morphology. (B) WT, *trappc11* mutants, and WT exposed to 0.5 µg/ml BFA were treated with increasing concentrations of Tm (1, 2, or 3 µg/ml) beginning at 3 dpf and scored for survival at 4 and 5 dpf (three clutches for each Tm concentration). WT, *trappc11* mutants, and BFA-treated samples are respectively represented by black, blue, and green lines, with 1, 2, and 3 µg/ml Tm indicated by solid, dashed, and dotted lines, respectively. (C) Cumulative survival at 5 dpf of WT, *trappc11* mutants, and WT + 0.5 µg/ml BFA exposed to Tm (1, 2, and 3 µg/ml) between 3 and 5 dpf. Black, blue, and green bars indicate WT, *trappc11*, and WT + BFA, respectively, with increased shading representing different clutches. Three clutches total were scored for survival. Gray segmented lines mark 100, 200, and 300% levels. (D) Livers from 5-dpf WT and *trappc11* mutants treated with DMSO or 0.125 µg/ml Tm were collected and subjected to qPCR analysis for UPR-responsive genes, and PC1 metrics were calculated. Values for each individual sample. (E) Livers from 5-dpf WT and *trappc11* mutants treated with DMSO, 0.25 µM thapsigargin, or 0.5 µM thapsigargin were collected and subjected to qPCR analysis for UPR-responsive genes, and PC1 metrics were calculated. The *p* values in C and D were calculated using Student's *t* test. n.s., not significant.

because the UPR pathway is enhanced by Tg but not by Tm, this suggests that the mechanism of UPR activation caused by *trappc11* mutation is in the same pathway targeted by Tm.

To further test our hypothesis that disruption of protein glycosylation activates the UPR more efficiently than a trafficking cargo backlog, we analyzed the data from a yeast genomic screen that measured UPR activity in ~5000 deletion mutants (Jonikas *et al.*, 2009). We performed spatial analysis of functional enrichment (SAFE; Baryshnikova, 2015) on the yeast genetic interaction similarity network (Supplemental Figure S4A, left; Costanzo *et al.*, 2010) to determine which biological functions, when mutated, caused the strongest up-regulation of UPR activity. As expected, we found that protein glycosylation mutants were the most effective at inducing the UPR (Supplemental Figure S4A). Mutations in vesicle-mediated transport pathways were also significantly involved, although the UPR response in these mutants was not as robust as that found with glycosylation mutants (Supplemental Figure S4A). Of note, only nonessential genes were examined, and thus only four TRAPP-complex genes were in the pool of mutants screened, and three of the four TRAPP-complex members present in the genetic interaction similarity network colocalized with the other vesicle transport genes in a network region that was significantly enriched for UPR upregulation (Supplemental Figure S4A). Furthermore, we asked whether in yeast, as in zebrafish, increased UPR activity correlated with increased sensitivity to Tm treatment (Supplemental Figure S4B). Using SAFE, we examined the data from a large-scale chemical genomic study (Parsons *et al.*, 2006) and found that mutations in protein folding and glycosylation, as well as vesicle-mediated trafficking, were highly enriched for Tm-sensitivity phenotypes (Supplemental Figure S4B). Although some trafficking factors are also Tm sensitive, the TRAPPs do not appear to be among the most highly synthetically lethal. These data are consistent with our finding that whereas *trappc11* zebrafish mutants do develop a defect in protein trafficking and this could account for an intermediate UPR, a trafficking defect is not sufficient to generate the robust, stressed UPR that causes fatty liver.

trappc11 mutation blocks protein N-linked glycosylation

On the basis of the foregoing data, we hypothesized that *trappc11*, like Tm, blocked protein

the vasculature. (D) Confocal images of livers from 5-dpf WT and *trappc11* mutants that express both the secreted Gc-EGFP (green) protein and the ER marker ER-tdTMT (red) confirms accumulation in the ER of mutant hepatocytes, evidenced by colocalization of both markers. (E) Western analysis of WT and *trappc11*-mutant livers using anti-GFP to detect Gc-EGFP and anti-Histone H3 as a loading control. Two independent clutches are shown for liver samples. Eight pooled livers and one liverless carcass were loaded. Bars, 10 µm (A, D).

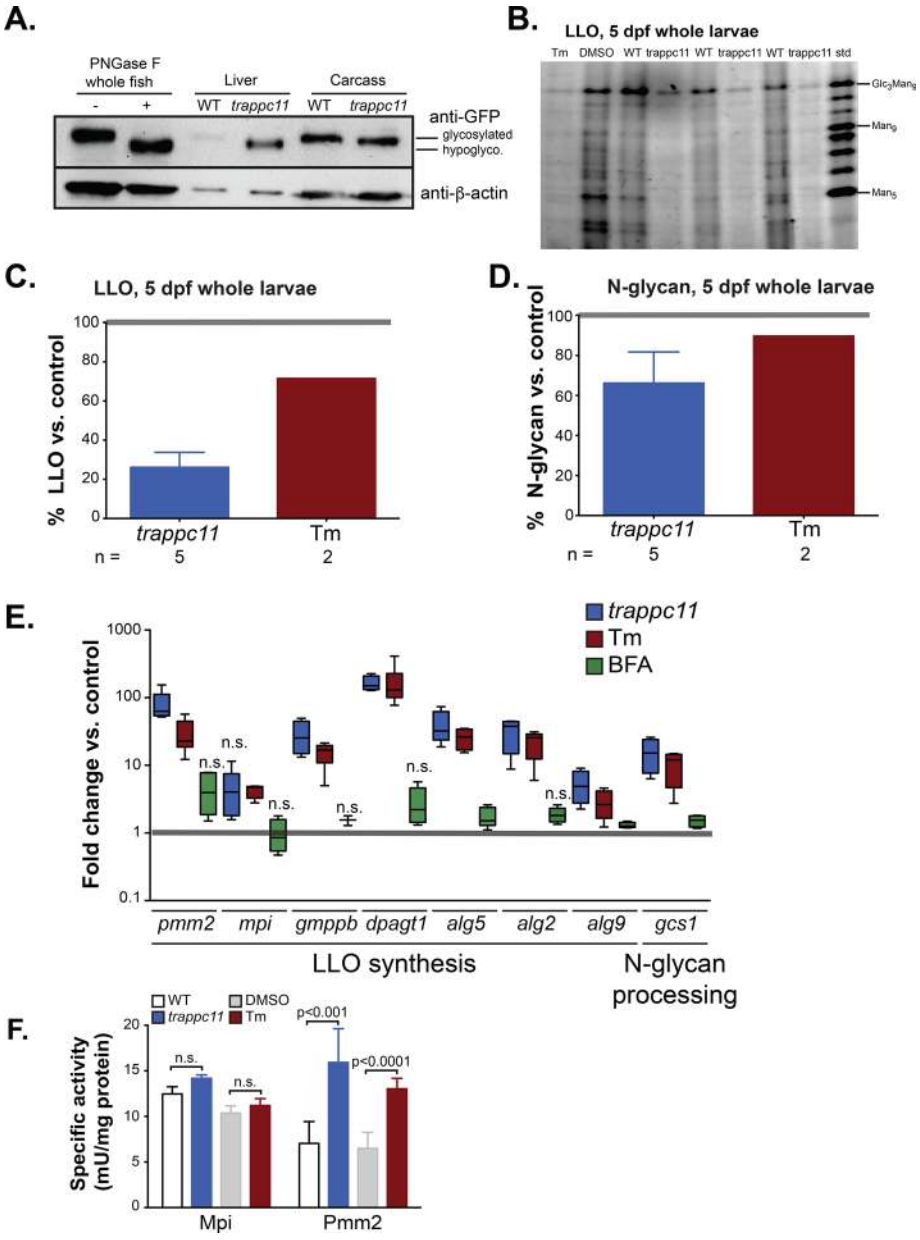

FIGURE 4: *trappc11* mutants have glycosylation defects. (A) Livers and liverless carcasses from *Tg(fabp10:Gc-EGFP)* WT and *trappc11* mutants at 5 dpf were collected and analyzed by Western blot for glycosylation of Gc-EGFP, with β-actin serving as a loading control. Blotting Gc-EGFP from WT whole-embryo lysates subjected to PNGase F digestion (+) serves as a control for hypoglycosylated Gc-EGFP. (B) LLO from 5-dpf WT and *trappc11* mutants, and WT larvae treated with 1 μg/ml Tm or DMSO, were purified and compared to DMSO-treated larvae analyzed by FACE. Standard marker separation (std) for size comparison is shown. (C) Amounts of full-length (Glc_3Man_9) LLO from B were quantified by ImageJ (National Institutes of Health, Bethesda, MD) densitometric analysis. *trappc11* mutants have ~25% LLO compared with WT siblings ($n = 5$). Tm treatment of WT embryos also results in reduced LLO levels ($n = 2$). (D) FACE analysis of N-linked glycans removed from proteins demonstrates that *trappc11* mutants ($n = 5$) have reduced glycosylation of proteins, also consistent with that seen in larvae treated with 1 μg/ml Tm ($n = 2$). Values in *trappc11* mutants were normalized to phenotypically WT siblings, and Tm-treated WT larvae were normalized to DMSO-treated controls. (E) Livers from WT siblings and *trappc11* mutants were collected and analyzed at 5 dpf for the expression of genes involved in N-linked glycosylation. Fold increases in expression was compared with WT siblings (for *trappc11*) or with DMSO-treated WT larvae for Tm and BFA-treated larvae (Tm and BFA-treated). There was significant up-regulation of genes involved in glycosylation in *trappc11* mutants (Student's *t* test). A similar increase is found in larvae treated with 1 μg/ml Tm, but not in those treated with 1 μg/ml BFA from 3 to 5 dpf. n.s., not significant. (F) Activity assays for Mpi and Pmm2 in 5 dpf WT and *trappc11*-mutant larvae. Tm-treated larvae (1 μg/ml) show comparable increase in Pmm2, but Mpi activity was not changed in *trappc11* in mutants or Tm-treated larvae. These changes are consistent with the gene expression shown in E. Mean ± SD of three independent clutches. The *p* values were calculated using Student's *t* test; n.s., not significant.

N-glycosylation. Differentially glycosylated forms of Gc-EGFP, which has three predicted glycosylation sites (NetGlyc 1.0; www.cbs.dtu.dk/services/NetNGlyc/), can be resolved by electrophoresis (Vacaru *et al.*, 2014a), as illustrated by the faster-migrating form detected in larvae treated with Tm (Vacaru *et al.*, 2014a) or in extracts from untreated WT *Tg(fabp10:Gc-EGFP)* larvae that were treated with peptide-*N*-glycosidase F (PNGase F) to completely remove N-glycans (Figure 4A). Gc-EGFP in the liver of *trappc11* mutants migrated faster than that from WT siblings (Figure 4A), consistent with a reduction in glycosylation. We found that Gc-EGFP in both WT and *trappc11*-mutant carcasses migrated at the same position as the fully glycosylated moiety (Figure 4A), indicating that some fully glycosylated Gc-EGFP is secreted in *trappc11* mutants. Treatment with endoglycosidase H (Endo H) to remove all high-mannose- containing residues, which characterize glycoproteins found in the ER, or with PNGase F, which removes all N-glycans, further increased the electrophoretic mobility of Gc-EGFP (Supplemental Figure S5A). We speculate that the trafficking defect in *trappc11* mutants causes secretory proteins to accumulate in the ER, and thus the mobility shift of Gc-EGFP in *trappc11* mutants may reflect both a reduction in glycosylation-site occupancy (producing a partial shift) and an accumulation of high-mannose-type glycans at some glycosylation sites.

We asked whether the glycosylation deficiency found with Gc-EGFP analysis in *trappc11* mutants was associated with a general reduction in LLO and N-glycans. We used fluorophore-assisted carbohydrate electrophoresis (FACE) analysis to compare the amount of full-length LLO and total N-linked glycans from 5-dpf WT and *trappc11* whole mutant larvae. $Glc_3Man_9GlcNAc_2$ LLO species (representative of full-length structures; Figure 4B) were significantly reduced to 26.2% of WT levels in *trappc11* mutants ($n = 4$, $p = 0.0003$; Figure 4C). Total N-glycans in mutants were lowered to 66.2% of that found in WT samples ($n = 5$, $p = 0.008$; Figure 4D and Supplemental Figure S5B). Within the working resolution of the

FACE gel (to Man_5-LLO), we did not detect abnormal accumulation of any truncated LLO intermediates, which might have also resulted in low efficiency of protein N-glycosylation. There was a similar but less pronounced reduction in both LLO (Figure 4, B and C) and total N-glycans (Figure 4D and Supplemental Figure S5B) in WT larvae treated with 1 μg/ml Tm from 3 to 5 dpf. Together these data lead to the surprising conclusion that *trappc11* mutation reduces both LLO levels and N-linked protein glycosylation and suggest that hypoglycosylation is the mechanism of stressed UPR induction.

To determine whether the LLO depletion in *trappc11* mutants could be accounted for by a change in the expression of genes required for LLO synthesis, we analyzed genes involved in the N-glycosylation biosynthetic pathway (*pmm2*, *mpi*, *gmppb*, *dpagt1*, *alg5*, *alg2*, and *alg9*) and one involved in N-glycan modification (*gcs1*) in the liver of *trappc11* mutants and compared their expression to that in larvae treated with Tm and BFA. Nearly all of these were up-regulated by >10-fold in 5-dpf *trappc11* mutant livers, and a similar pattern was observed in livers of larvae exposed to Tm (Figure 4E). Of interest, *dpagt1*, whose protein product is the target of Tm, was the most up-regulated gene in both *trappc11* and Tm samples. The high expression of *pmm2* in *trappc11* and Tm-treated larvae was also reflected in an increase in the resultant phosphomannomutase 2 (Pmm2) enzyme activity (Figure 4F). However, mannose phosphate isomerase (Mpi), a protein involved in fructose and mannose metabolism, was not induced at the mRNA or protein (enzymatic) level in the liver of either Tm-treated larvae or *trappc11* mutants (Figure 4, E and F). Furthermore, BFA treatment had little effect on the expression of any gene regulating protein glycosylation (Figure 4E). The striking similarity in the gene expression profile of *trappc11* mutants and larvae treated with Tm suggests that the block in protein glycosylation in both of these models results in a compensatory up-regulation of genes involved in LLO synthesis in an attempt to overcome LLO deficiency.

trappc11 mutation regulates terpenoid and dolichol synthesis pathways

On the basis of the forgoing findings, we hypothesized that *trappc11* mutation could be affecting either dolichol phosphate synthesis or an upstream step in the pathway that leads to dolichol synthesis. Farnesyl-pyrophosphate (PP) is produced by the terpenoid synthesis pathway (also known as the HMG-CoA or mevalonate pathway; Figure 5A) and is a key precursor for four important products: 1) dolichol-PP, 2) cholesterol, 3) geranylgeranyl-PP, which together with farnesyl-PP is used for the prenylation of proteins, and 4) ubiquinone.

We tested whether *trappc11*-mutant livers had alterations in the expression of genes encoding enzymes in the terpenoid (Figure 5A and Supplemental Figure S6A) and the dolichol synthesis pathway (Figure 5A and Supplemental Figure S6, A and B). Figure 5A shows all of the enzymes involved in the mevalonate pathway, the dolichol synthesis pathway, and a subset of those involved in LLO synthesis, with red and blue indicating genes that were up- or down-regulated, respectively, whereas genes in white boxes showed no change in *trappc11* mutants (gray boxes indicate genes that were not analyzed). This analysis revealed a striking pattern of up-regulation of nearly all genes involved in dolichol synthesis, including *dhdds* and *srd5a3*, which convert farnesyl-PP to dehydrodolichol-PP and dolichol, respectively. Up-regulation was also seen for *dpm1*, *2*, and *3*, whose products form a complex that generates mannose-P-dolichol, the substrate used for addition of mannose to LLOs in the ER lumen and for O-glycosylated proteins (Figure 5A and Supplemental Figure S6, A and B). The most highly up-regulated gene in this pathway was *dpagt1* (Figures 4E and 5A), which encodes the enzyme that links dolichol to GlcNAc and is the target of Tm. Moreover, nearly all other genes examined that participate in the LLO synthesis pathway, including those that modify mannose (*pmm2*, *gmppb*) and those that function to elongate the oligosaccharide chain (*alg5*, *alg2*, *alg9*), were highly and significantly up-regulated in *trappc11*-mutant livers (Figures 4E and 5A).

To determine whether the decreased levels of LLO found in *trappc11* mutants is due to a general repression of the terpenoid biosynthetic pathway, we analyzed the outcomes of other arms of this pathway: protein prenylation and cholesterol. To examine protein prenylation, we used a transgenic zebrafish line in which hepatocytes express GFP fused to a CAAX motif, which is a substrate for prenylation and thus becomes localized to the plasma membrane (*Tg(fabp10:CAAX-GFP)*; Jacob *et al.*, 2015). In contrast to WT siblings, in which CAAX-GFP was primarily membrane localized in hepatocytes (Figure 5B) and gut epithelial cells (Supplemental Figure S6C), in *trappc11*-mutant cells, some GFP was retained in the cytoplasm, appearing to be diffuse, as well as in punctate and aggregated foci (Figure 5B). This accumulation pattern of CAAX-GFP in *trappc11* mutants was likely not to be secondary to the secretion defect, since treating WT control zebrafish with 0.75 μg/ml BFA did not result in CAAX-GFP accumulation in a similar manner, despite development of membrane blebbing (Figure 5C). Furthermore, whereas GFP was entirely static in WT hepatocytes (Supplemental Movie S1), the intracellular GFP-labeled punctae in *trappc11* mutants were highly mobile (Supplemental Movie S2), suggesting that they may have aggregated or be associated with a motile structure. Although we are unsure of the identity of these structures, their increased abundance in *trappc11* mutants is highly suggestive of reduced protein prenylation.

We next measured cholesterol levels in extracts from WT and *trappc11*-mutant 5-dpf whole larvae to determine whether cholesterol synthesis was affected in *trappc11* mutants. Overall *trappc11* mutants had a modest (14.4%) but statistically significant reduction of cholesterol compared with WT siblings, with 14 of 17 clutches examined having lower levels of cholesterol in mutants (paired *t* test, $p = 0.0008$, $n = 17$ clutches; Figure 5D). Of interest, *fdft1* (also called squalene synthase), which converts farnesyl-PP to squalene, is down-regulated in *trappc11*-mutant livers (Figure 5A and Supplemental Figure S6B). We speculate that this may serve as a compensatory mechanism to increase flux to the dolichol pathway and could account for the moderate decrease in cholesterol levels detected in *trappc11* mutants.

Atorvastatin causes a stressed UPR

On the basis of the foregoing gene expression patterns and reduction in both cholesterol and protein prenylation, we hypothesized that the stressed UPR in *trappc11* mutants could be attributed to a decrease in the terpenoid biosynthetic pathway. We tested this hypothesis by treating larvae with atorvastatin (Atv). Statins inhibit HMG-CoA reductase (HMGCR) and are among the most highly used pharmaceuticals worldwide because they reduce cholesterol by blocking production of mevalonate (Figure 5A). WT larvae treated between 3 and 5 dpf tolerated exposure to 1 μM Atv and developed only mild phenotypic defects with 5 μM exposure (Figure 6A). *trappc11* mutants were sensitized to Atv, as they all died with 5 μM exposure and were severely affected with 1 μM (Figure 6A). Reduced liver size was observed in *trappc11* mutants treated with 1 μM Atv, which we attribute to adverse effects on liver development. Thus, blocking mevalonate synthesis is synthetically lethal with the *trappc11* mutation, indicating that they act in the same pathway.

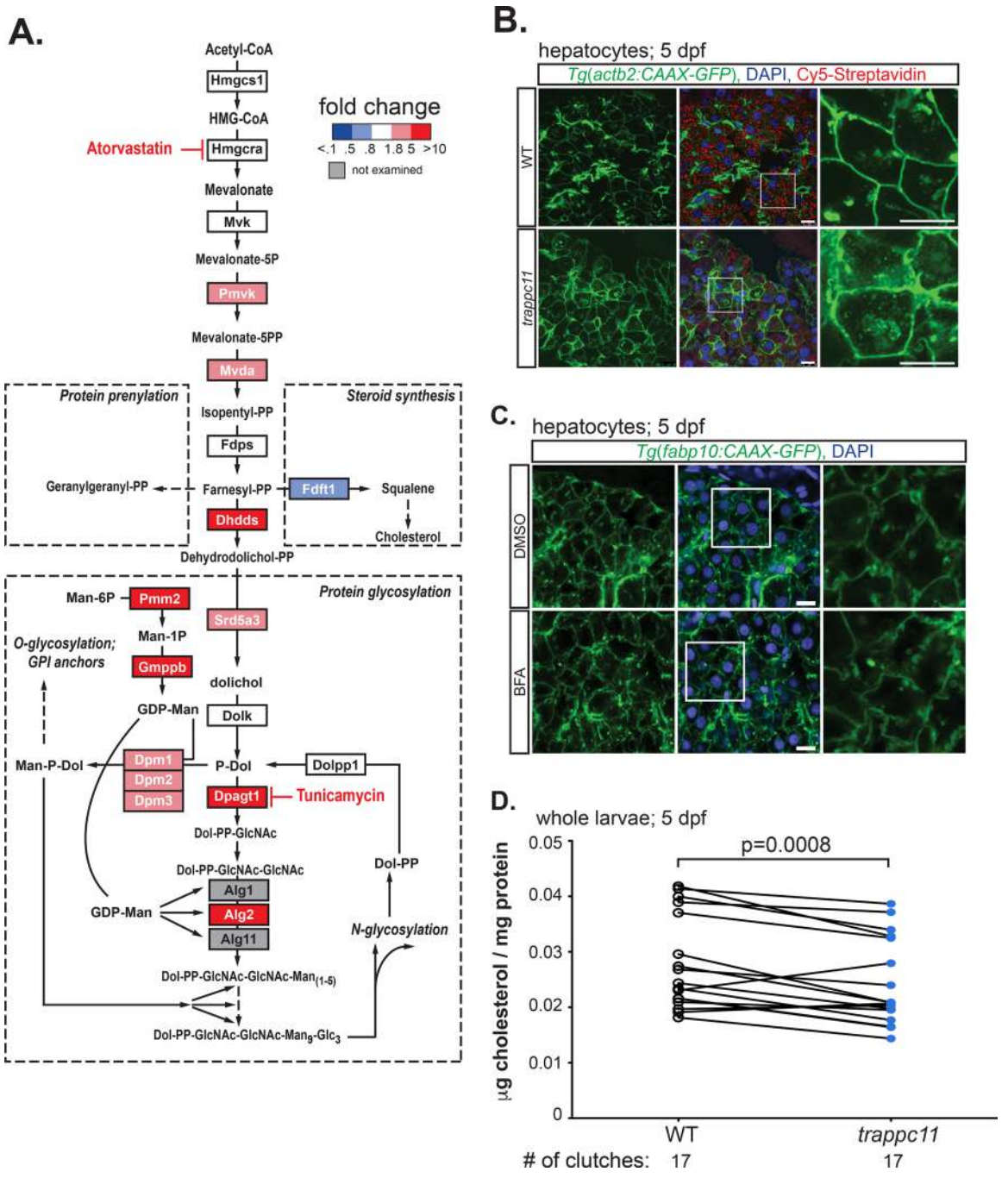

FIGURE 5: Terpenoid and dolichol synthesis defects in *trappc11* mutants. (A) Schematic representation of the terpenoid biosynthetic pathway, with branch points at farnesyl-PP leading to production of dolichol (protein glycosylation), squalene (steroid synthesis), and geranylgeranyl-PP (protein prenylation). Fold changes of expression in *trappc11* mutant livers are indicated by color: blue indicates decrease and red indicates increase relative to WT siblings; gray indicates genes not tested. Drugs used are indicated with a red T at their targets. (B) Confocal microscopy of transgenic WT and *trappc11*-mutant zebrafish expressing a prenylated form of GFP (*Tg(actb2:CAAX-GFP)*) in hepatocytes. Zebrafish were collected at 5 dpf and analyzed for membrane localization of CAAX-GFP. Samples were counterstained with DAPI (nucleus) and Cy5-streptavidin to stain the biotin-rich hepatocytes (middle; white boxes outline magnified GFP-only images shown on right). Scale bars, 10 µm. (C) Confocal microscopy of WT transgenic zebrafish expressing a prenylated form of GFP in hepatocytes (*Tg(fabp10:CAAX-GFP)*. Zebrafish larvae were treated with DMSO (top) or 0.75 µg/ml BFA (bottom) from 3 to 5 dpf and analyzed at 5 dpf for membrane localization of CAAX-GFP. Samples were counterstained with DAPI (blue nucleus). White boxes outline area shown magnified on right (GFP only). Scale bars, 10 µM. (D) Whole WT and *trappc11*-mutant larvae were collected at 5 dpf, and total cholesterol was measured and normalized to protein content. *trappc11* mutants have a significant decrease in cholesterol compared with WT siblings ($p = 0.0008$, paired Student's *t* test), suggestive of decreased terpenoid biosynthetic activity. Individual clutches are indicated ($n = 17$ for each), with lines representing clutch pairing.

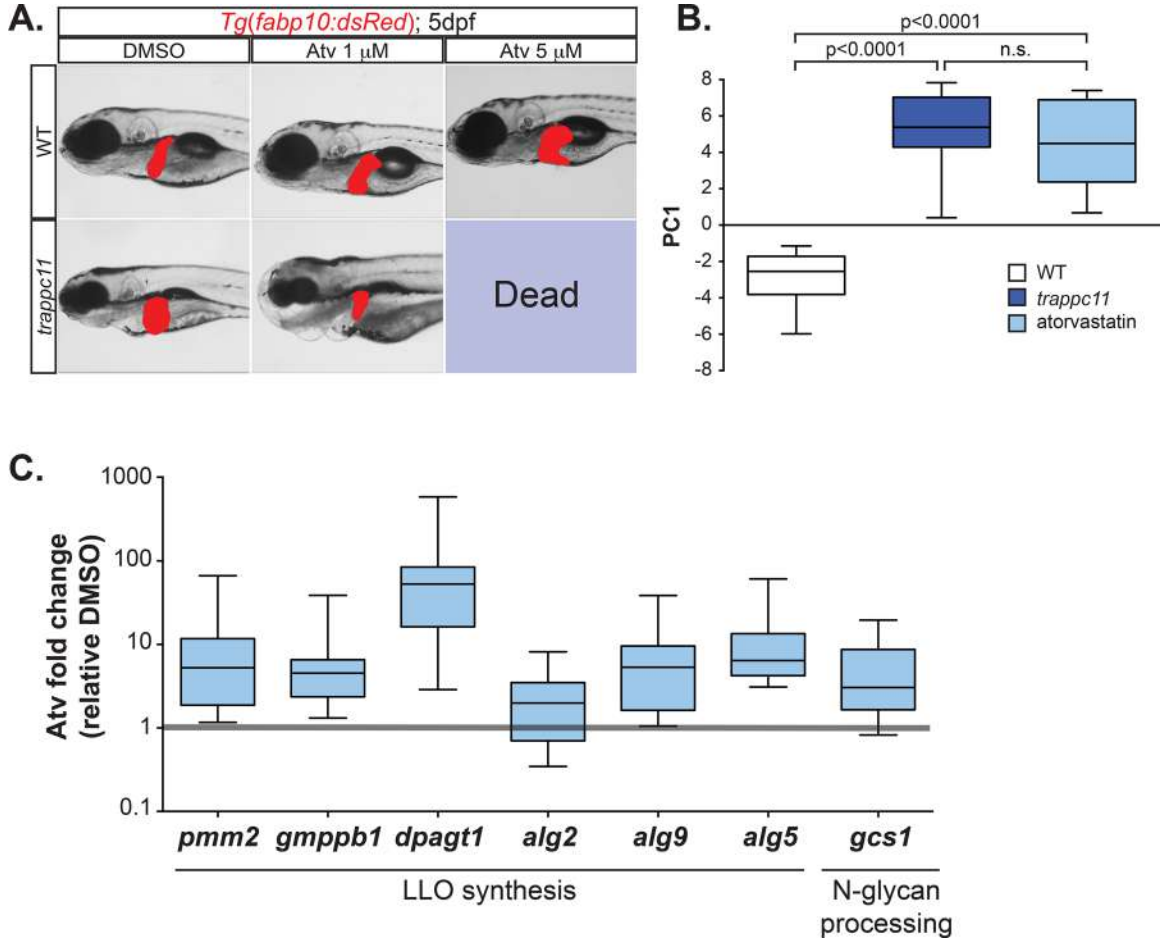

FIGURE 6: Atorvastatin is synthetically lethal with *trappc11* mutation. (A) Transgenic WT and *trappc11*-mutant embryos expressing a liver-specific marker (*Tg(fabp10:dsRed)*) were treated with DMSO or the HMG-CoA reductase inhibitor, Atv, between 3 and 5 dpf at the concentrations indicated and analyzed for gross morphology and lethality. (B) Livers were collected from WT ($n = 7$ clutches), *trappc11* ($n = 8$ clutches), and 5 μM Atv–treated WT embryos between 3 and 5 dpf ($n = 7$ clutches) and subjected to qPCR to analyze UPR gene expression used to calculate PC1. *p* values were calculated with Student's *t* test. n.s., not significant. (C) Livers from larvae treated with DMSO or 1 μM Atv from 3 to 5 dpf ($n = 8$ clutches) were collected and analyzed at 5 dpf for the expression of genes involved in N-linked glycosylation. Atorvastatin-induced fold increases are shown relative to DMSO-treated samples.

We hypothesized that Atv would reduce glycosylation by lowering dolichol levels and subsequently induce a stressed UPR. Atv treatment of WT larvae caused significant up-regulation of UPR target genes (Supplemental Figure S7), with PC1 similar to that detected in *trappc11* mutant livers at 5 dpf (Figure 6B). In addition, Atv treatment induced the expression of genes in LLO synthesis (Figure 6C). Thus, blocking terpenoid synthesis is sufficient to phenocopy *trappc11* mutation.

TRAPPC11 loss in human cells results in defective protein glycosylation and lipid accumulation

We next asked whether loss of TRAPPC11 in human cells could also cause protein hypoglycosylation. We examined glycosylation by assessing the mobility of signal sequence receptor α (SSR1; also called translocon-associated protein α [TRAPα]) in HeLa cells transfected with small interfering RNA (siRNA) targeting *TRAPPC11* and three other genes encoding TRAPP-complex proteins (Figure 7, A and B). As previously shown, *TRAPPC11* siRNA transfection caused fragmentation of the Golgi complex (Supplemental Figure S8A) but did not have a marked effect on the structure of the ER (Supplemental Figure S8B). Despite the similarity in name, TRAPα is distinct from the TRAPP complex and is part of an ER-resident complex involved in calcium binding to the ER membrane to promote retention of proteins (Wu *et al.*, 2007; Supplemental Figure S8A). TRAPα has two glycosylation sites whose glycans are not processed in the Golgi, making it an ideal glycosylation marker to detect site occupancy defects. Remarkably, 48 h after *TRAPPC11* siRNA transfection, TRAPα displayed two additional moieties with increased electrophoretic mobility compared with cells transfected with a nontargeting control siRNA (indicated by asterisk in Figure 7A). These forms represent unglycosylated and monoglycosyated TRAPα. By 72 h, all TRAPα had become completely unglycosylated, producing a single band with electrophoretic mobility identical to samples treated with Endo H (Figure 7A). Of importance, knockdown of TRAPPC8, TRAPPC12, or TRAPPC2 had no effect on glycosylation of TRAPα (Figure 7A) even though the siRNA-mediated depletion of these factors was efficient (Figure 7B). These results demonstrate that the requirement for TrappC11 for glycosylation is conserved across vertebrates and is specific to TRAPPC11 depletion and not a general response to disruption of the TRAPP complex.

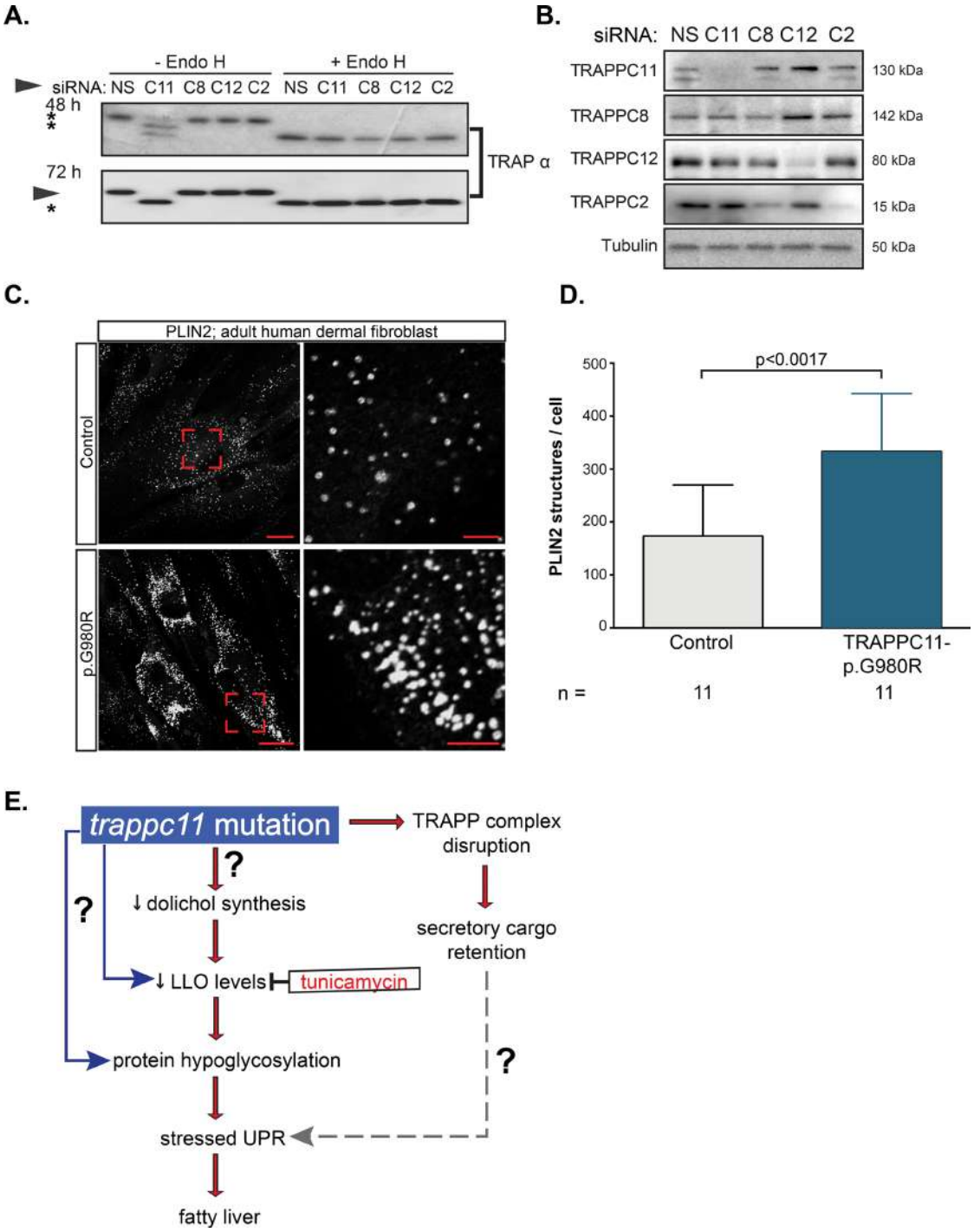

FIGURE 7: TRAPPC11 in human cells is required for glycosylation and for inhibiting lipid accumulation. (A) HeLa cells were transfected with either a nonspecific siRNA (NS) or siRNA targeting *TRAPPC11* (C11), *TRAPPC8* (C8), *TRAPPC12* (C12), or *TRAPPC2* (C2) transcripts and probed after 48 and 72 h for glycosylation of the ER-resident protein TRAPα. Asterisks indicate hypoglycosylated (unglycosylated and monoglycosylated) moieties of TRAPα. Representative Western blot of three experiments. Endo H digestion was performed to indicate fully hypoglycosylated high-mannose-containing species. (B) siRNA-mediated knockdown of TRAPP components shown in A were confirmed by Western blot using antibodies against TRAPPC11, TRAPPC8, TRAPPC12, and TRAPPC2. Tubulin was used as a loading control. Molecular size of TRAPP members is shown on the right. (C) Dermal fibroblasts from control or a patient harboring the homozygous missense mutation p.G980R in TRAPPC11 were fixed and stained with anti-PLIN2 antibody, followed by Alexa Fluor 647. Scale bars, 25 μm (left), 5 μm (right). The images are representative of three independent experiments. (D) Quantification of the PLIN2-positive structures per cell confirms a significant increase in PLIN2-positive structures in p.G980R patient cells compared with control cells (Student's *t* test). Number of cells counted (*n*) is indicated. (E) Working model for mechanism by which *trappc11* mutation causes a stressed UPR and fatty liver. Both protein glycosylation and protein trafficking are blocked in *trappc11* mutants, and our data suggest that the protein glycosylation defect, either alone or with the added cellular stress caused by secretory cargo retention, leads to a stressed UPR, which causes fatty liver.

The most striking phenotype of *trappc11*-mutant zebrafish is the large liver, in which hepatocytes accumulate lipid (Sadler *et al.*, 2005; Cinaroglu *et al.*, 2011). We examined fibroblasts from patients bearing a homozygous point mutation changing glycine 980 to arginine (p.G980R), resulting in decreased protein levels (Bogershausen *et al.*, 2013). Glycine 980 is highly conserved and located within the N-terminal Gryzun domain, which has an unknown function. Patient fibroblasts also accumulated lipid, as determined by immunofluorescence with perilipin 2, which serves to coat intracellular lipid droplets. The analysis of the images revealed that fibroblasts from the *TRAPPC11*-mutation patient had more-abundant lipid droplets than did fibroblasts from controls (Figure 7, C and D). Thus the phenotypes of zebrafish and human cells with *TRAPPC11* mutations are similar.

DISCUSSION

The causes of fatty liver disease range from alcohol abuse, to type II diabetes, to inborn errors of metabolism, and most etiologies of fatty liver are associated with activation of the UPR (Imrie and Sadler, 2012; Wang and Kaufman, 2014). We found that only a robust, stressed UPR can cause fatty liver disease (Cinaroglu *et al.*, 2011; Vacaru *et al.*, 2014a) by activating the main UPR mediator, Atf6 (Cinaroglu *et al.*, 2011; Howarth *et al.*, 2014). We sought to understand how this disease-causing UPR can become activated by identifying the mechanism of UPR activation in zebrafish *trappc11* mutants that spontaneously develop both a stressed UPR and fatty liver (Sadler *et al.*, 2005; Cinaroglu *et al.*, 2011). We made the unexpected finding that, in addition to the predicted defects in protein secretion due to TRAPP-complex dysfunction, *trappc11* mutants also have a defect in protein N-glycosylation. Collectively our data suggest a model (Figure 7E) in which *trappc11* mutation blocks LLO formation, leading to the accumulation of hypoglycosylated proteins. This would trigger a stressed UPR, including Atf6 activation leading to fatty liver. Of importance, our findings in human cells suggest that similar mechanisms may underlie the *trappc11*-mutant zebrafish phenotype and could contribute to the pathophysiology of patients with *TRAPPC11* mutation.

The role of the TRAPP complex in vesicle trafficking has been well studied in yeast, in which different versions of the complex function as a Rab guanine nucleotide exchange factor. This facilitates vesicle trafficking from the ER to the Golgi complex, trafficking within the Golgi stacks, and autophagosome formation (Lipatova *et al.*, 2015). TRAPPC11 is highly conserved in metazoans but not in yeast, and we found that the Golgi complex becomes fragmented in *trappc11*-mutant cells in zebrafish, similar to that reported in insect (Wendler *et al.*, 2010) and human (Scrivens *et al.*, 2011; Bogershausen *et al.*, 2013) cells with TRAPPC11 depletion. In vertebrates, conserved TRAPP-complex proteins likely serve similar functions as their yeast counterparts. However, there are additional complex members in vertebrates, and the function of these proteins is only beginning to be understood. Several studies have uncovered functions for TRAPP-complex proteins in an array of cellular processes other than vesicle trafficking (Bassik *et al.*, 2013; Rybak *et al.*, 2014; Milev *et al.*, 2015). Our studies suggest that, in addition to the role in maintaining TRAPP-complex integrity, TRAPPC11 may also function to regulate N-linked glycosylation.

The analysis here describes several defects in *trappc11* mutants. Mutants have defects in protein secretion from hepatocytes and marked fragmentation of the Golgi complex, similar to the phenotype in insect and mammalian cells depleted of the respective *trappc11* homologues (Wendler *et al.*, 2010; Scrivens *et al.*, 2011; Bassik *et al.*, 2013). Because of the unique association between the distinct stressed UPR subclass and fatty liver, we are most interested in identifying how this UPR subclass can be activated. We tested the hypothesis that a backlog of secretory cargo produced by the trafficking defect in *trappc11* mutants caused a stressed UPR but found that complete disruption of the Golgi complex using BFA, inducing severe secretory protein retention in hepatocytes (Figure 2C), was insufficient to induce a robust UPR or fatty liver (Vacaru *et al.*, 2014a). Thus we concluded that a block in protein trafficking cannot be the only cause of the stressed UPR in *trappc11* mutants.

Our enrichment analysis on UPR activation in yeast deletion mutants identified statistical associations with protein folding and glycosylation pathways in addition to vesicle-mediated transport (Supplemental Figure S4A). However, of the >100 genes that, when deleted, induced the UPR, no TRAPP-complex members or its main target, Ypt1 (the Rab1 homologue in yeast; Jonikas *et al.*, 2009), was identified as substantially inducing the UPR. Instead, many genes required for protein glycosylation (*ALG3*, *ALG5*, *ALG6*, *ALG8*, *ALG9*, *ALG12*, *OST3*) and for dolichol synthesis (*DIE2*) were on the list of hits that induced the UPR when deleted (Jonikas *et al.*, 2009). Of interest, among the most robust inducers was *ARV1*, a gene required for sterol metabolism (Tinkelenberg *et al.*, 2000). This supports a model in which blocking terpenoid synthesis and the subsequent reduction in dolichol levels is a potent stress that induces the UPR.

On the basis of the similarity in morphological and cellular phenotypes between *trappc11* mutants and WT larvae treated with Tm, as well as their similar gene expression profiles (Figures 1, 4E, and 5A; Cinaroglu *et al.*, 2011; Vacaru *et al.*, 2014a), we reasoned that the mechanism inducing the stressed UPR was the same between these two models. Our data demonstrate that *trappc11* mutants have a defect in protein glycosylation and a reduction in LLOs and N-glycans, which supports this conclusion. Moreover, our finding that *trappc11* mutants have up-regulated the genes encoding enzymes that control the entire dolichol synthesis pathway and that they are sensitized to a reduction in the mevalonate pathway further supports this hypothesis.

Although the effects on protein prenylation and cholesterol were relatively mild in *trappc11* mutants compared with the effect on protein glycosylation and it is possible that *trappc11* mutation could cause these defects by an indirect mechanism, our data are nevertheless consistent with the hypothesis that *trappc11* mutation reduces farnesyl-PP availability. The combined reduction in LLO production, protein prenylation, and cholesterol synthesis in *trappc11* mutants suggests a model in which the terpenoid biosynthetic pathway is impaired by *trappc11* mutation, leading to a defect in either the generation of farnesyl-PP or its subsequent processing to dolichol-PP. This in turn results in reduced LLOs, protein hypoglycosylation, and activation of a stressed UPR, which causes fatty liver.

A role for a TRAPP-complex member in pathways other than vesicle trafficking has been suggested by previous studies. For example, the TRAPP complex plays a prominent role in autophagosome formation in yeast, and a mammalian screen to enlarge the autophagy protein network identified TRAPPC11 as a member of this network that was separate from the other TRAPP proteins that were identified in a complex in this screen (Behrends *et al.*, 2010). Although it is feasible that a block in autophagy in *trappc11* mutants could contribute to the UPR and lipid accumulation, there is no evidence that the autophagy pathway interacts with the protein glycosylation pathway, and thus it is unclear whether this is directly relevant to the LLO depletion and Tm and Atv sensitivity observed in these mutants. Previous studies showed that TRAPPC2 is a transcriptional regulator (Ghosh *et al.*, 2001, 2003) and that TRAPPC9 regulates NF-κB signaling through a role independent of the TRAPP

complex (Mir *et al.*, 2009; Philippe *et al.*, 2009). A recent study identified a moonlighting role for another TRAPP complex member (TRAPPC12/TRAMM) in chromosome segregation (Milev *et al.*, 2015), which is completely separate from its function in vesicle trafficking. These studies set a precedent for other TRAPP-complex factors, such as TRAPPC11, to play roles in cellular processes other than membrane trafficking.

Our working model is that mutation of TRAPPC11 reduces dolichol levels by blocking production of farnesyl-PP, dolichol, or its derivatives (Figure 7E). Although the specific mechanism by which *trappc11* mutation leads to protein hypoglycosylation is not known, one possibility is that TRAPPC11 functions as a scaffold for enzymes in this pathway, analogous to its role as a scaffold in the TRAPP complex (Scrivens *et al.*, 2011; Bassik *et al.*, 2013). Another possibility is that TRAPPC11 functions as a cofactor for one of the enzymes in LLO synthesis. Our data suggest that Tm and *trappc11* mutation target the same process, and it is intriguing to speculate that TRAPPC11 is a regulator of DPAGT1; limitations in TRAPPC11 abundance could explain the paradoxical observation that only a minor fraction of overexpressed DPAGT1 in mammalian cells is actually functional in LLO synthesis (Gao and Lehrman, 2002; Gao *et al.*, 2008). A third possibility is that LLO depletion is caused not by impaired synthesis but by enhanced destruction. LLO cleavage can be caused by high levels of Man-6-P, which accumulates during UPR activation, releasing free glycans and P-Dol (Gao *et al.*, 2011). A pilot study did not detect elevated Man-6-P levels in *trappc11* mutants, suggesting this as less likely. Identifying the biochemical mechanism by which *trappc11* mutation reduces protein glycosylation is an important goal for future studies.

The relevance of this study to human disease was recently highlighted by reports that patients with mutations in *TRAPPC11* develop limb girdle muscular dystrophy and intellectual disability (Bogershausen *et al.*, 2013). Patients with similar symptoms have been reported, and many of these are caused by a defect in protein glycosylation. For example, one such set of patients has a mutation in *GMPPB*, which is required for LLO synthesis (Carss *et al.*, 2013). We observed motility defects in *trappc11*-mutant larvae (K.C.S. and R.R., unpublished data), similar to zebrafish lacking *gmppb* (Carss *et al.*, 2013), and we are investigating this phenotype further to determine whether it is due to an abnormality in muscle development or function. We speculate that the clinical syndrome in patients with *TRAPPC11* mutation may be attributed to a deficit in the dolichol substrate required for glycosylation of proteins. Our finding of a requirement for TRAPPC11 in protein glycosylation in human cells and the recent report of a patient with *TRAPPC11* mutation presenting with fatty liver (Liang *et al.*, 2015) highlight the importance of our findings to human disease.

MATERIALS AND METHODS

Zebrafish maintenance

WT (TAB14 and ABNYU) and mutant lines (*trappc11*^{hi1532b}) were maintained in accordance with the policies of the Mount Sinai Institutional Animal Care and Use Committee. Mutants were genotyped as described (Amsterdam *et al.*, 2004). *Tg(fabp10:RFP;ela:GFP)* fish were obtained from D. Stainier (University of California, San Francisco, San Francisco, CA), and *Tg(fabp10:Gc-EGFP)* and *Tg(actb2:GalT-GFP)* were previously described by Xie *et al.* (2010) and Gerhart *et al.* (2011), respectively. Transgenic lines expressing the fluorescent organelle markers for the ER and for the plasma membrane, *Tg(fabp10:ER-tdTomato)*, *Tg(actb2:CAAX-GFP)*, and *Tg(fabp10:CAAX-GFP)*, were obtained by injecting the corresponding construct into the one-cell-stage zebrafish embryos. At 3 dpf, the embryos were screened for the expression of the transgene in the expected tissue and cell compartment and then raised until adulthood to create the founders of the line. These were then outcrossed with TAB14 WT, and progeny expressing the transgene were raised and crossed to *trappc11*-mutant heterozygotes. Throughout the study, we used F2 and F3 generations of *Tg(fabp10:ER-tdTomato)*, *Tg(actb2:CAAX-GFP)*, *Tg(fabp10:CAAX-GFP)*, and *Tg(actb2:GalT-EGFP)*. All of the transgenics in the *trappc11* background were obtained by outcrossing *Tg(fabp10:ER-tdTomato)*, *Tg(fabp10:Gc-EGFP)*, *Tg(actb2:CAAX-GFP)*, *Tg(fabp10:CAAX-GFP)*, and *Tg(actb2:GalT-GFP)* to *trappc11* heterozygotes. The progeny were genotyped, and the heterozygotes carrying the transgene were raised to adulthood.

Drug treatments

Zebrafish *trappc11* mutants and their phenotypically WT siblings were treated from 3 to 5 dpf with different concentrations, as indicated, of BFA, Tm, Tg, or Atv dissolved in dimethyl sulfoxide (DMSO). Equal volumes of DMSO were used to treat siblings and used as a control. At 5 dpf, mutant larvae were identified based on their morphological phenotype (Sadler *et al.*, 2005) and processed according to the corresponding assay.

Western blotting

For zebrafish samples, 10–30 livers from 5 dpf transgenic *Tg(fabp10:Gc-EGFP)* embryos were dissected, pooled, and immunoblotted with an anti-GFP antibody (Invitrogen, Carlsbad, CA) as described (Vacaru *et al.*, 2014a). As a control for the band shift, PNGase-treated (New England Biolabs, Ipswich, MA) whole WT embryos were used as described (Vacaru *et al.*, 2014a). Tubulin (Sigma-Aldrich, Allentown, PA) and Histone H3 (Santa Cruz Biotechnology, Dallas, TX) were used for loading controls. For analysis of *trappc11* mutation, whole 5 dpf WT sibling and *trappc11*-mutant larvae were separated by SDS–PAGE and probed with a custom antibody against zebrafish Trappc11 (see the Supplemental Data).

For human samples, HeLa cells were cultured in DMEM supplemented with 10% fetal calf serum. At 40% confluency, the cells were transfected with siRNA targeting TRAPPC11 (5′-GGAUUUAUAAACUACAAGGATT-3′), TRAPPC2 (5′-UCCAUUUUAUGAACCCAAUTT-3′), TRAPPC8 (5′-CAGCUCUCCUAAUACGGUUTT-3′), TRAPPC12 (5′-CGGACAAGCUGAACGAACATT-3′), or nonspecific siRNA (5′-UAACGACGCGACGACGUAATT-3′) as described (Milev *et al.*, 2015) at a final concentration of 60 nM for 48 and 72 h using JetPrime (Polyplus) as per the manufacturer's protocol. Transfected cells were lysed, and 20 µg lysate was treated with 5 U of either Endo H (New England Biolabs) or PNGase F at 37°C for 1 h as per manufacturer suggestions. Samples were separated by SDS–PAGE and probed with antibodies against human TRAPα (kind gift from Ramanujan Hegde, MRC Laboratory of Molecular Biology, Cambridge, United Kingdom), TRAPPC11 (Scrivens *et al.*, 2011), TRAPPC2 (Scrivens *et al.*, 2009), TRAPPC8 (Abcam, Cambridge, United Kingdom), TRAPPC12 (Milev *et al.*, 2015), or mouse tubulin (Sigma-Aldrich).

qPCR

Real-time qPCR was performed as described (Vacaru *et al.*, 2014a). Briefly, 10–25 livers from 5-dpf larvae were dissected and pooled in RLT Lysis Buffer (Qiagen, Hilden, Germany). RNA extraction was performed using TRIzol (Invitrogen). cDNA was generated using the qScript cDNA SuperMix kit (Quanta BioSciences, Gaithersburg, MD), and qPCR was performed using PerfeCTa SYBR Green FastMix (Quanta BioSciences) paired with the primers listed in Supplemental Table S1.

Cholesterol and enzyme assays

Cholesterol was measured using the Cholesterol Assay Kit (Biovision, Milpitas, CA) following the manufacturer's instructions. Briefly, whole 5-dpf larvae were lysed in 0.5% Triton X-100 (VWR, Radnor, PA) by sonication. After clarification of the lysate by centrifugation, the supernatant was diluted with cholesterol buffer and then incubated with enzyme mix, cholesteryl esterase enzyme, and a probe for 1 h at 37°C. The samples were analyzed at 570 nm. Cholesterol levels were normalized to the total protein concentration as determined by Bradford assay (Thermo Fisher Scientific, Waltham, MA).

Pmm2 and Mpi enzyme activity assays were carried out as described (Chu *et al.*, 2013).

LLO and N-glycan analysis

LLOs and N-glycans were extracted and analyzed by FACE in three separate clutches of 100 larvae from each genotype as described (Chu *et al.*, 2013).

Cell imaging and data analysis

To detect changes in the hepatic ER and Golgi complex, *Tg(fabp10:ER-tdTomato;fabp10:Gc-EGFP)* or *Tg(fabp10:ER-tdTomato;actb2:GalT-GFP)* larvae were fixed in 4% paraformaldehyde (PFA) in phosphate-buffered saline (PBS) for 24 h and infused in 30% sucrose before mounting in optimum cutting temperature (OCT; Sakura) medium. Ten-micrometer cryosections were prepared on a Leica CM 3050S cryostat and mounted with Vectashield containing 4′,6-diamidino-2-phenylindole (DAPI; Vector Laboratories, Burlingame, CA). Confocal sections were obtained using a Leica SP5 DM confocal microscope with a 63×/numerical aperture (NA) 1.4 oil objective.

A single section was used to analyze the ER and stacks composed of five to seven optical sections to analyze Golgi apparatus morphology. In each field, the total number of transgene-expressing cells was counted based on the DAPI staining. The ER in each cell was scored as normal if it displayed a reticular pattern or abnormal if it displayed distended, vesiculated, or globular structures. The Golgi apparatus was scored as abnormal if the structure lost the characteristic compactness of the Golgi ribbon, displayed disruption in evenly or unevenly sized vesicles, expansion of the structure, or haziness. Between 198 and 437 hepatocytes were counted in different fields from 8–14 larvae collected from at least two different clutches.

Immunofluorescence of fibroblasts from patients with a homozygous mutation (p.G980R) in TRAPPC11 (Bogershausen *et al.*, 2013) and WT controls were grown in DMEM supplemented with 10% fetal bovine serum for 24 h. Cells were fixed in 3% PFA, washed in PBS, and permeabilized and blocked in 1× PBS, 0.1 mg/ml saponin, 0.5 mg/ml BSA, and 0.2 M glycine. Polyclonal rabbit anti-PLIN2 antibody (Abcam, Cambridge, MA) and Alexa Fluor 647 secondary goat anti-rabbit (Life Technologies, Carlsbad, CA) were used, and cells were mounted in Prolong Gold AntiFade reagent (Life Technologies) for imaging. Images of 2048 × 2048–pixel resolution were recorded on a Nikon Laser scanning confocal microscope C2 fitted with a 63× Plan Apo I, NA 1.4 objective (Nikon, Tokyo, Japan) controlled by NIS-Elements C 4.3 software. Optical sections were acquired with a 0.2-µm increment.

Z-stacks of 1 µm were exported to Imaris, version 8.1 (Bitplane, Zürich, Switzerland), for identification and calculation of all PLIN2-labeled structures in manually selected, three-dimensionally rendered cells. The analysis was performed on 11 random cells over three experiments. Unpaired two-tailed *t* tests with Welch's correction, assuming unequal SD, were performed to estimate significant differences between means using Prism (GraphPad Software, La Jolla, CA).

ACKNOWLEDGMENTS

This work was supported by National Institutes of Health Grant R01 AA018886 (to K.C.S.) and Grant R01 DK099551 (to H.H.F.), the Rocket Fund (to H.H.F.), and R01 GM038545 (to M.L.) and the Canadian Institutes of Health Research, Natural Sciences and Engineering Research Council of Canada (M.S.). M.S. is a member of the Groupe de Recherche Axé sur la Structure des Protéines network. We thank E. Closser, M. Nash, and P. Bradley for expert fish care and F. Oltrabella for technical support.

REFERENCES

Amsterdam A, Nissen RM, Sun Z, Swindell EC, Farrington S, Hopkins N (2004). Identification of 315 genes essential for early zebrafish development. Proc Natl Acad Sci USA 101, 12792–12797.

Barrowman J, Bhandari D, Reinisch K, Ferro-Novick S (2010). TRAPP complexes in membrane traffic: convergence through a common Rab. Nat Rev Mol Cell Biol 11, 759–763.

Baryshnikova A (2015). Systematic functional annotation and visualization of biological networks. bioRxiv doi: 10.1101/030551.

Bassik MC, Kampmann M, Lebbink RJ, Wang S, Hein MY, Poser I, Weibezahn J, Horlbeck MA, Chen S, Mann M, *et al.* (2013). A systematic mammalian genetic interaction map reveals pathways underlying ricin susceptibility. Cell 152, 909–922.

Behrends C, Sowa ME, Gygi SP, Harper JW (2010). Network organization of the human autophagy system. Nature 466, 68–76.

Bogershausen N, Shahrzad N, Chong JX, von Kleist-Retzow JC, Stanga D, Li Y, Bernier FP, Loucks CM, Wirth R, Puffenberger EG, *et al.* (2013). Recessive TRAPPC11 mutations cause a disease spectrum of limb girdle muscular dystrophy and myopathy with movement disorder and intellectual disability. Am J Hum Genet 93, 181–190.

Carss KJ, Stevens E, Foley AR, Cirak S, Riemersma M, Torelli S, Hoischen A, Willer T, van Scherpenzeel M, Moore SA, *et al.* (2013). Mutations in GDP-mannose pyrophosphorylase B cause congenital and limb-girdle muscular dystrophies associated with hypoglycosylation of alpha-dystroglycan. Am J Hum Genet 93, 29–41.

Chu J, Mir A, Gao N, Rosa S, Monson C, Sharma V, Steet R, Freeze HH, Lehrman MA, Sadler KC (2013). A zebrafish model of congenital disorders of glycosylation with phosphomannose isomerase deficiency reveals an early opportunity for corrective mannose supplementation. Dis Model Mech 6, 95–105.

Cinaroglu A, Gao C, Imrie D, Sadler KC (2011). Activating transcription factor 6 plays protective and pathological roles in steatosis due to endoplasmic reticulum stress in zebrafish. Hepatology 54, 495–508.

Costanzo M, Baryshnikova A, Bellay J, Kim Y, Spear ED, Sevier CS, Ding H, Koh JL, Toufighi K, Mostafavi S, *et al.* (2010). The genetic landscape of a cell. Science 327, 425–431.

Gao N, Lehrman MA (2002). Coupling of the dolichol-P-P-oligosaccharide pathway to translation by perturbation-sensitive regulation of the initiating enzyme, GlcNAc-1-P transferase. J Biol Chem 277, 39425–39435.

Gao N, Shang J, Huynh D, Manthati VL, Arias C, Harding HP, Kaufman RJ, Mohr I, Ron D, Falck JR, *et al.* (2011). Mannose-6-phosphate regulates destruction of lipid-linked oligosaccharides. Mol Biol Cell 22, 2994–3009.

Gao N, Shang J, Lehrman MA (2008). Unexpected basis for impaired Glc3Man9GlcNAc2-P-P-dolichol biosynthesis by elevated expression of GlcNAc-1-P transferase. Glycobiology 18, 125–134.

Gedeon AK, Colley A, Jamieson R, Thompson EM, Rogers J, Sillence D, Tiller GE, Mulley JC, Gecz J (1999). Identification of the gene (SEDL) causing X-linked spondyloepiphyseal dysplasia tarda. Nat Genet 22, 400–404.

Gerhart SV, Eble DM, Burger RM, Oline SN, Vacaru A, Sadler KC, Jefferis R, Iovine MK (2012). The Cx43-like connexin protein Cx40.8 is differentially localized during fin ontogeny and fin regeneration. PLoS One 7, e31364.

Ghosh AK, Majumder M, Steele R, White RA, Ray RB (2001). A novel 16-kilodalton cellular protein physically interacts with and antagonizes the functional activity of c-myc promoter-binding protein 1. Mol Cell Biol 21, 655–662.

Ghosh AK, Steele R, Ray RB (2003). Modulation of human luteinizing hormone beta gene transcription by MIP-2A. J Biol Chem 278, 24033–24038.
Howarth DL, Lindtner C, Vacaru AM, Sachidanandam R, Tsedensodnom O, Vasilkova T, Buettner C, Sadler KC (2014). Activating transcription factor 6 is necessary and sufficient for alcoholic fatty liver disease in zebrafish. PLoS Genet 10, e1004335.
Howarth DL, Yin C, Yeh K, Sadler KC (2013). Defining hepatic dysfunction parameters in two models of fatty liver disease in zebrafish larvae. Zebrafish 10, 199–210.
Imrie D, Sadler KC (2012). Stress management: how the unfolded protein response impacts fatty liver disease. J Hepatol 57, 1147–1151.
Jacob V, Chernyavskaya Y, Chen X, Tan PS, Kent B, Hoshida Y, Sadler KC (2015). DNA hypomethylation induces a DNA replication-associated cell cycle arrest to block hepatic outgrowth in uhrf1 mutant zebrafish embryos. Development 142, 510–521.
Jonikas MC, Collins SR, Denic V, Oh E, Quan EM, Schmid V, Weibezahn J, Schwappach B, Walter P, Weissman JS, *et al.* (2009). Comprehensive characterization of genes required for protein folding in the endoplasmic reticulum. Science 323, 1693–1697.
Lehrman MA, Zhu XY, Khounlo S (1988). Amplification and molecular cloning of the hamster tunicamycin-sensitive N-acetylglucosamine-1-phosphate transferase gene. The hamster and yeast enzymes share a common peptide sequence. J Biol Chem 263, 19796–19803.
Liang W-C, Zhu W, Mitsuhashi S, Noguchi S, Sacher M, Ogawa M, Shi HH, Jong YH, Nishino I (2015). Congenital muscular dystrophy with fatty liver and infantile-onset cataract caused by TRAPPC11 mutations: broadening of the phenotype. Skelet Muscle 5, 29.
Lipatova Z, Hain AU, Nazarko VY, Segev N (2015). Ypt/Rab GTPases: principles learned from yeast. Crit Rev Biochem Mol Biol 50, 203–211.
Milev MP, Hasaj B, Saint-Dic D, Snounou S, Zhao Q, Sacher M (2015). TRAMM/TrappC12 plays a role in chromosome congression, kinetochore stability, and CENP-E recruitment. J Cell Biol 209, 221–234.
Mir A, Kaufman L, Noor A, Motazacker MM, Jamil T, Azam M, Kahrizi K, Rafiq MA, Weksberg R, Nasr T, *et al.* (2009). Identification of mutations in TRAPPC9, which encodes the NIK- and IKK-beta-binding protein, in nonsyndromic autosomal-recessive mental retardation. Am J Hum Genet 85, 909–915.
Oakes SA, Papa FR (2015). The role of endoplasmic reticulum stress in human pathology. Annu Rev Pathol 10, 173–194.
Parsons AB, Lopez A, Givoni IE, Williams DE, Gray CA, Porter J, Chua G, Sopko R, Brost RL, Ho CH, *et al.* (2006). Exploring the mode-of-action of bioactive compounds by chemical-genetic profiling in yeast. Cell 126, 611–625.
Philippe O, Rio M, Carioux A, Plaza JM, Guigue P, Molinari F, Boddaert N, Bole-Feysot C, Nitschke P, Smahi A, *et al.* (2009). Combination of linkage mapping and microarray-expression analysis identifies NF-kappaB signaling defect as a cause of autosomal-recessive mental retardation. Am J Hum Genet 85, 903–908.
Rutkowski DT, Kaufman RJ (2007). That which does not kill me makes me stronger: adapting to chronic ER stress. Trends Biochem Sci 32, 469–476.
Rybak K, Steiner A, Synek L, Klaeger S, Kulich I, Facher E, Wanner G, Kuster B, Zarsky V, Persson S, *et al.* (2014). Plant cytokinesis is orchestrated by the sequential action of the TRAPPII and exocyst tethering complexes. Dev Cell 29, 607–620.
Sadler KC, Amsterdam A, Soroka C, Boyer J, Hopkins N (2005). A genetic screen in zebrafish identifies the mutants vps18, nf2 and foie gras as models of liver disease. Development 132, 3561–3572.
Scrivens PJ, Noueihed B, Shahrzad N, Hul S, Brunet S, Sacher M (2011). C4orf41 and TTC-15 are mammalian TRAPP components with a role at an early stage in ER-to-Golgi trafficking. Mol Biol Cell 22, 2083–2093.
Tinkelenberg AH, Liu Y, Alcantara F, Khan S, Guo Z, Bard M, Sturley SL (2000). Mutations in yeast ARV1 alter intracellular sterol distribution and are complemented by human ARV1. J Biol Chem 275, 40667–40670.
Vacaru AM, Di Narzo AF, Howarth DL, Tsedensodnom O, Imrie D, Cinaroglu A, Amin S, Hao K, Sadler KC (2014a). Molecularly defined unfolded protein response subclasses have distinct correlations with fatty liver disease in zebrafish. Dis Model Mech 7, 823–835.
Vacaru AM, Unlu G, Spitzner M, Mione M, Knapik EW, Sadler KC (2014b). In vivo cell biology in zebrafish—providing insights into vertebrate development and disease. J Cell Sci 127, 485–495.
Wang S, Kaufman RJ (2014). How does protein misfolding in the endoplasmic reticulum affect lipid metabolism in the liver? Curr Opin Lipidol 25, 125–132.
Wendler F, Gillingham AK, Sinka R, Rosa-Ferreira C, Gordon DE, Franch-Marro X, Peden AA, Vincent JP, Munro S (2010). A genome-wide RNA interference screen identifies two novel components of the metazoan secretory pathway. EMBO J 29, 304–314.
Wu J, Rutkowski DT, Dubois M, Swathirajan J, Saunders T, Wang J, Song B, Yau GD, Kaufman RJ (2007). ATF6alpha optimizes long-term endoplasmic reticulum function to protect cells from chronic stress. Dev Cell 13, 351–364.
Xie J, Farage E, Sugimoto M, Anand-Apte B (2010). A novel transgenic zebrafish model for blood-brain and blood-retinal barrier development. BMC Dev Biol 10, 76.

Supplemental Materials

Molecular Biology of the Cell

DeRossi et al.

Supplementary Information

Supplementary Materials and Methods

Generation of zebrafish-specific Trappc11 N-terminal antibody

A polyclonal antibody against the N-terminus of zebrafish Trappc11 was developed in rabbits by immunizing with the epitope KVLPGDHEYPKCRTKR, corresponding to amino acids 54 to 69 of the zebrafish Trappc11 protein. This epitope is encoded within exon 2, and is expected to detect the full length protein (129 kDa) in addition to other splice variants, and also to detect a predicted ~59 kDa product from the truncated protein expressed by the *trappc11*^{hi1532b} mutant allele.

Immunofluorescence

HeLa cells transfected with siRNA targeting TRAPPC11, or non-targeting control siRNA, were collected 48 hours after transfection and stained with antibodies recognizing TRAPα, the Golgi complex protein p115 (kind gift from Dennis Shields, Albert Einstein College of Medicine, New York, USA) and the ER chaperone calnexin (kind gift from John Bergeron, McGill University, Montreal, Canada) and counterstained with DAPI to label the nucleus.

Live imaging

Live 5 dpf *trappc11* mutants or their phenotypically WT siblings with Tg(fabp10:CAAX-GFP) were mounted in 0.5% low melt agarose and imaged at 30 second intervals for 5 minutes using a 60X oil immersion objective with a 1.5X zoom on a Zeiss LSM-780 confocal microscope. Movies are representative of the 3-4 embryos observed per genotype.

Spatial Analysis of Functional Enrichment (SAFE)

The data measuring UPR regulation were downloaded from the Supplementary Table 1 of the original publication (Jonikas *et al.*, 2009) in the form of average GFP/RFP reporter ratios. The chemical genomic data for Tm were downloaded from the Supplementary Table 7 of the original publication (Parsons *et al.*, 2006) in the

form of raw log2 barcode hybridization ratios. Spatial Analysis of Functional Enrichment (SAFE) was performed with default parameters as described in (Baryshnikova, 2015).

Supplementary Figure Legends

Figure S1. Trappc11 protein is affected in *trappc11* mutants

WT control, siblings (sibs) and *trappc11* mutant whole larvae were collected at 5 dpf, and lysates were separated by SDS-PAGE and probed using an antibody against the N-terminal region of zebrafish Trappc11. The full length (129 kDa) Trappc11 protein and the *foigr* protein (predicted to be ~56 kDa) from *trappc11* mutants are indicated. Molecular weight standard sizes are shown on left. Tubulin was used as loading control.

Figure S2. Tm induces a stressed UPR.

WT zebrafish embryos were treated with DMSO (n=6) or 1 μg/ml Tm (n=7) between 3 to 5 dpf, and livers were collected at 5 dpf for qPCR analysis. A gene panel of 8 UPR responsive genes was analyzed and demonstrates induction of a stressed UPR following Tm exposure.

Figure S3. UPR induction persists in *trappc11* mutants during development.

(A) WT and *trappc11* mutant transgenic zebrafish harboring a liver-specific fluorescent marker (*Tg(fabp10:dsRed)*) were collected at 3, 4 and 5 dpf and analyzed for overt morphological abnormalities. At 3 dpf, *trappc11* mutants are comparable to WT siblings, but at 4 and 5 dpf progressive hepatomegaly is observed in *trappc11* mutants. Genotyping PCR results are shown with WT and *trappc11* indicated. **(B)** qPCR analysis of the UPR response gene panel reveals that at 3 dpf, a stressed UPR is present in both WT and *trappc11* mutants, that is resolved in WT siblings but persists in *trappc11* mutants at 4 and 5 dpf (Figure 1). Box and whisker plots are shown for 3 clutches.

Figure S4. Spatial Analysis of Functional Enrichment (SAFE) of the UPR program in yeast.

(**A**) The yeast genetic interaction similarity network connects genes that share similar genetic interaction profiles and likely act in related biological processes (Costanzo *et al.*, 2010). Spatial Analysis of Functional Enrichment (SAFE) determines which regions of the network are overrepresented for a quantitative phenotype of interest and therefore uncovers statistical associations between phenotypes and underlying biological processes (Baryshnikova, 2015) . Using the data from a quantitative genome-wide screen that examined UPR activity in ~5,000 yeast deletion mutants (Jonikas *et al.*, 2009), SAFE showed that mutations in protein folding and glycosylation, as well as vesicle-mediated transport pathways, cause an up-regulation of the UPR program. Network localization of members of the TRAPP protein complex and the N-glycosylation pathway is shown with respect to the affected network regions. (**B**) Chemical genomic data from genome-wide mutant screens (Parsons *et al.*, 2006) were examined with SAFE in a similar manner. Mutants that show resistance or sensitivity to a chemical compound are highly indicative of the compound's mode-of-action (Ho *et al.*, 2011; Roemer *et al.*, 2012). SAFE showed that, consistently with the up-regulation of UPR activity, mutations in protein folding and glycosylation were the most sensitive to Tm and some of the genes involved in protein trafficking were also synthetically lethal with Tm.

Figure S5. *trappc11* mutants have reduced glycosylation.

(A) Livers from *Tg(fabp10:Gc-EGFP)* WT and *trappc11* mutants at 5 dpf were collected and analyzed by Western blot for glycosylation of Gc-EGFP. Samples were subjected to Endo H or PNGase F digestion to detect high-mannose and all N-glycan modifications, respectively. Differing exposure times were necessary to clearly show digestions from both WT sibling and *trappc11* mutant samples. **(B)** N-glycans were prepared by PNGase F digestion, from 5 dpf WT and *trappc11* mutants, or WT embryos treated with DMSO or 1 μg/ml Tm, and subjected to FACE analysis. Two

WT and 3 *trappc11* mutant samples are shown, and a single sample for DMSO and Tm-treatment. Decreased total N-glycans are found in *trappc11* mutants, compared to WT siblings, a pattern similar to that seen with Tm treatment. Glucose standards (G4, G5, G6 and G7) were used for structure sizing and identification. Typically, G6 standard runs slightly slower than the released N–linked heptasaccharide $Man_5GlcNAc_2$.

Figure S6. Terpenoid pathway response in *trappc11* mutants.

(A and B) Livers from WT and *trappc11* mutant zebrafish (6 clutches) were collected at 5 dpf, pooled and analyzed by qPCR for genes involved in the terpenoid biosynthetic pathway (A) and glycosylation and cholesterol synthesis (B). dCt values, relative to *rpp0*, are shown. Asterisks indicate a statistically significant change in dCt compared to WT siblings ($p<0.05$, Student's t-test). **(C)** WT and *trappc11* mutant transgenic zebrafish (*Tg(actb2:CAAX-GFP)*) were analyzed at 5 dpf for membrane localization in the gut of a CAAX-GFP prenylation marker. *trappc11* mutants have increased cytosolic mislocalization of CAAX-GFP away from the plasma membrane. Samples were counterstained for DAPI (blue) and Cy5-Streptavidin (red). Scale bars are 10 μm.

Figure S7. Atorvastatin induces the UPR in zebrafish liver.

WT zebrafish larvae were treated with DMSO or 5 μM atorvastatin (Atv) between 3 to 5 dpf, and livers were collected at 5 dpf and analyzed by qPCR for a panel of 8 UPR response genes (7 clutches).

Figure S8. TRAPPC11 depletion causes fragmentation of the GC and does not affect localization of TRAP alpha.

(A and B) Fluorescence microscopy of HeLa cells transfected with a non-specific siRNA (NS) or treated with 60 nM siRNA targeting *TrappC11* (C11 KD) for 48 hours, fixed and stained with anti-TRAP and anti-p115 (**A**) or anti-calnexin and anti-p115

(**B**). The merged images include DAPI staining to reveal the nucleus. Scale bars are 20 μm.

Supplemental References

Baryshnikova, A. (2015). Systematic Functional Annotation and Visualization of Biological Networks. bioRxiv.

Costanzo, M., Baryshnikova, A., Bellay, J., Kim, Y., Spear, E.D., Sevier, C.S., Ding, H., Koh, J.L., Toufighi, K., Mostafavi, S., Prinz, J., St Onge, R.P., VanderSluis, B., Makhnevych, T., Vizeacoumar, F.J., Alizadeh, S., Bahr, S., Brost, R.L., Chen, Y., Cokol, M., Deshpande, R., Li, Z., Lin, Z.Y., Liang, W., Marback, M., Paw, J., San Luis, B.J., Shuteriqi, E., Tong, A.H., van Dyk, N., Wallace, I.M., Whitney, J.A., Weirauch, M.T., Zhong, G., Zhu, H., Houry, W.A., Brudno, M., Ragibizadeh, S., Papp, B., Pal, C., Roth, F.P., Giaever, G., Nislow, C., Troyanskaya, O.G., Bussey, H., Bader, G.D., Gingras, A.C., Morris, Q.D., Kim, P.M., Kaiser, C.A., Myers, C.L., Andrews, B.J., and Boone, C. (2010). The genetic landscape of a cell. Science *327*, 425-431.

Ho, C.H., Piotrowski, J., Dixon, S.J., Baryshnikova, A., Costanzo, M., and Boone, C. (2011). Combining functional genomics and chemical biology to identify targets of bioactive compounds. Curr Opin Chem Biol *15*, 66-78.

Jonikas, M.C., Collins, S.R., Denic, V., Oh, E., Quan, E.M., Schmid, V., Weibezahn, J., Schwappach, B., Walter, P., Weissman, J.S., and Schuldiner, M. (2009). Comprehensive characterization of genes required for protein folding in the endoplasmic reticulum. Science *323*, 1693-1697.

Parsons, A.B., Lopez, A., Givoni, I.E., Williams, D.E., Gray, C.A., Porter, J., Chua, G., Sopko, R., Brost, R.L., Ho, C.H., Wang, J., Ketela, T., Brenner, C., Brill, J.A., Fernandez, G.E., Lorenz, T.C., Payne, G.S., Ishihara, S., Ohya, Y., Andrews, B., Hughes, T.R., Frey, B.J., Graham, T.R., Andersen, R.J., and Boone, C. (2006). Exploring the mode-of-action of bioactive compounds by chemical-genetic profiling in yeast. Cell *126*, 611-625.

Roemer, T., Davies, J., Giaever, G., and Nislow, C. (2012). Bugs, drugs and chemical genomics. Nat Chem Biol *8*, 46-56.

Supplemental Figure S1

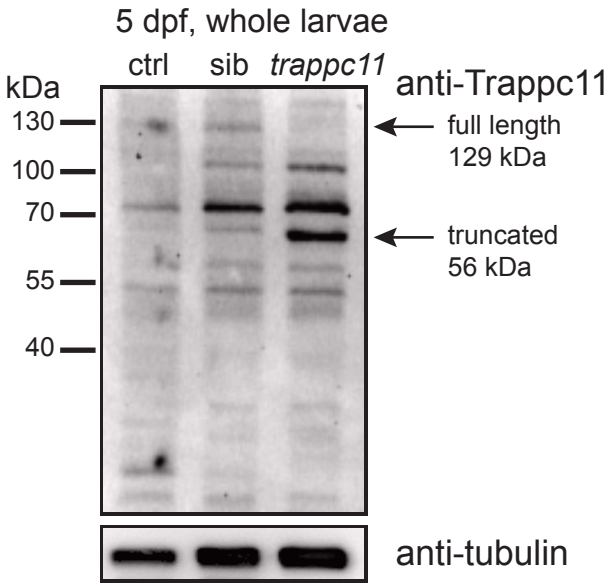

Supplemental Figure S2

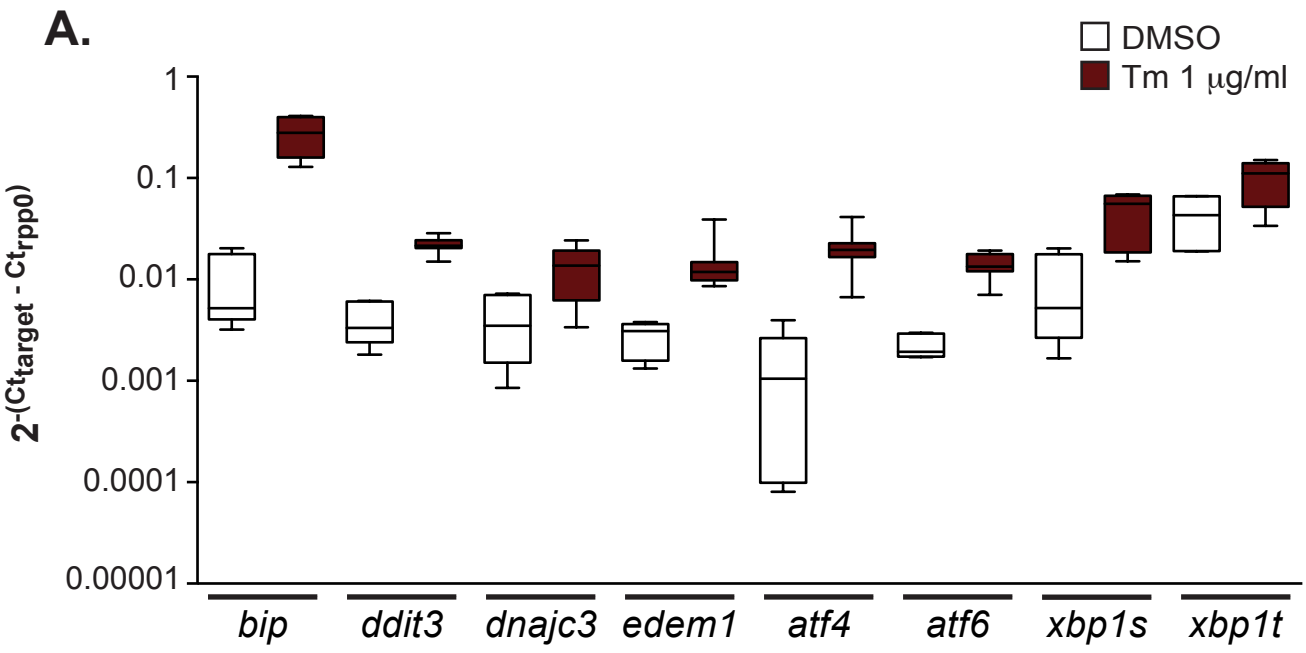

Supplemental Figure S3

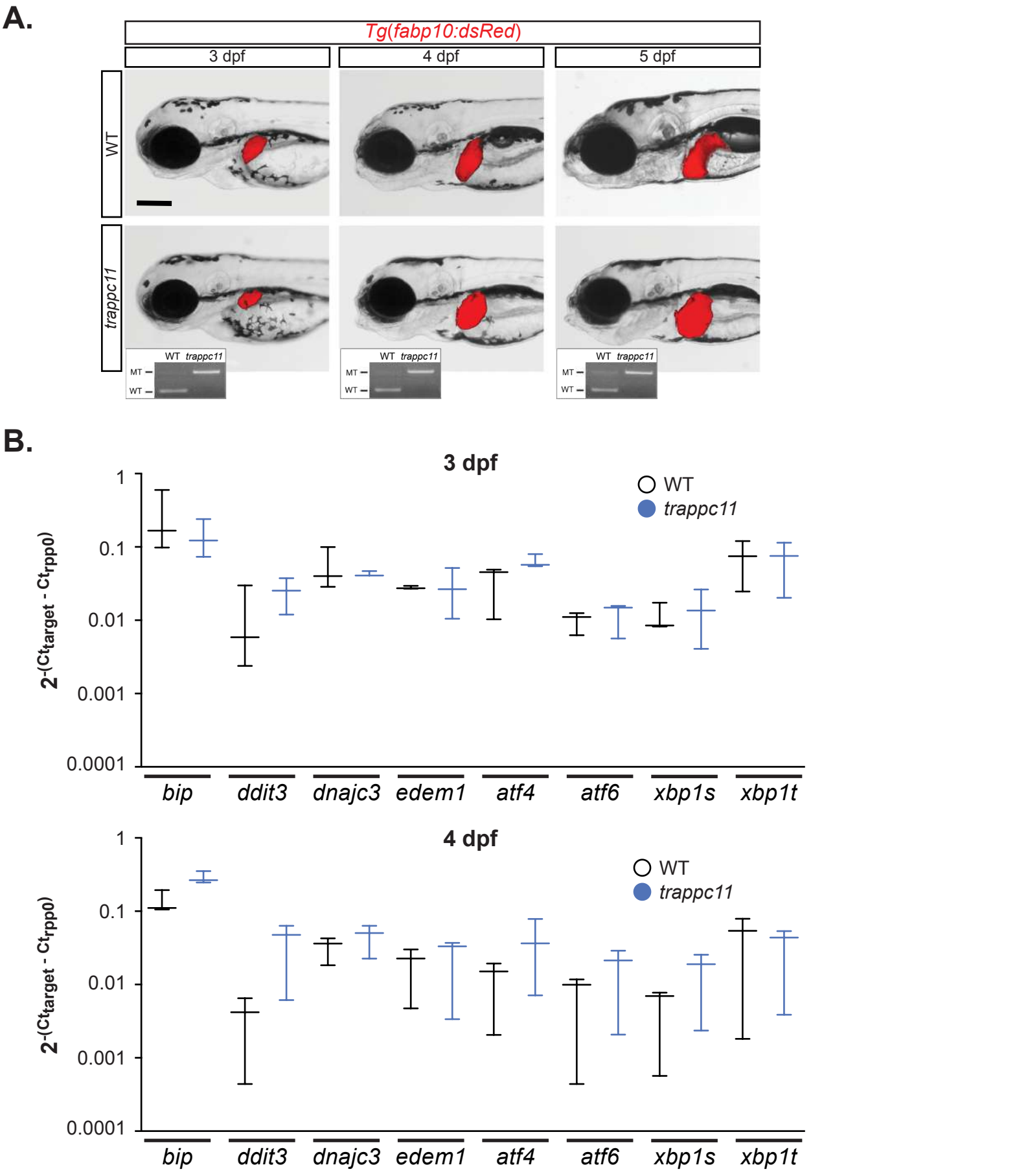

Supplemental Figure S4

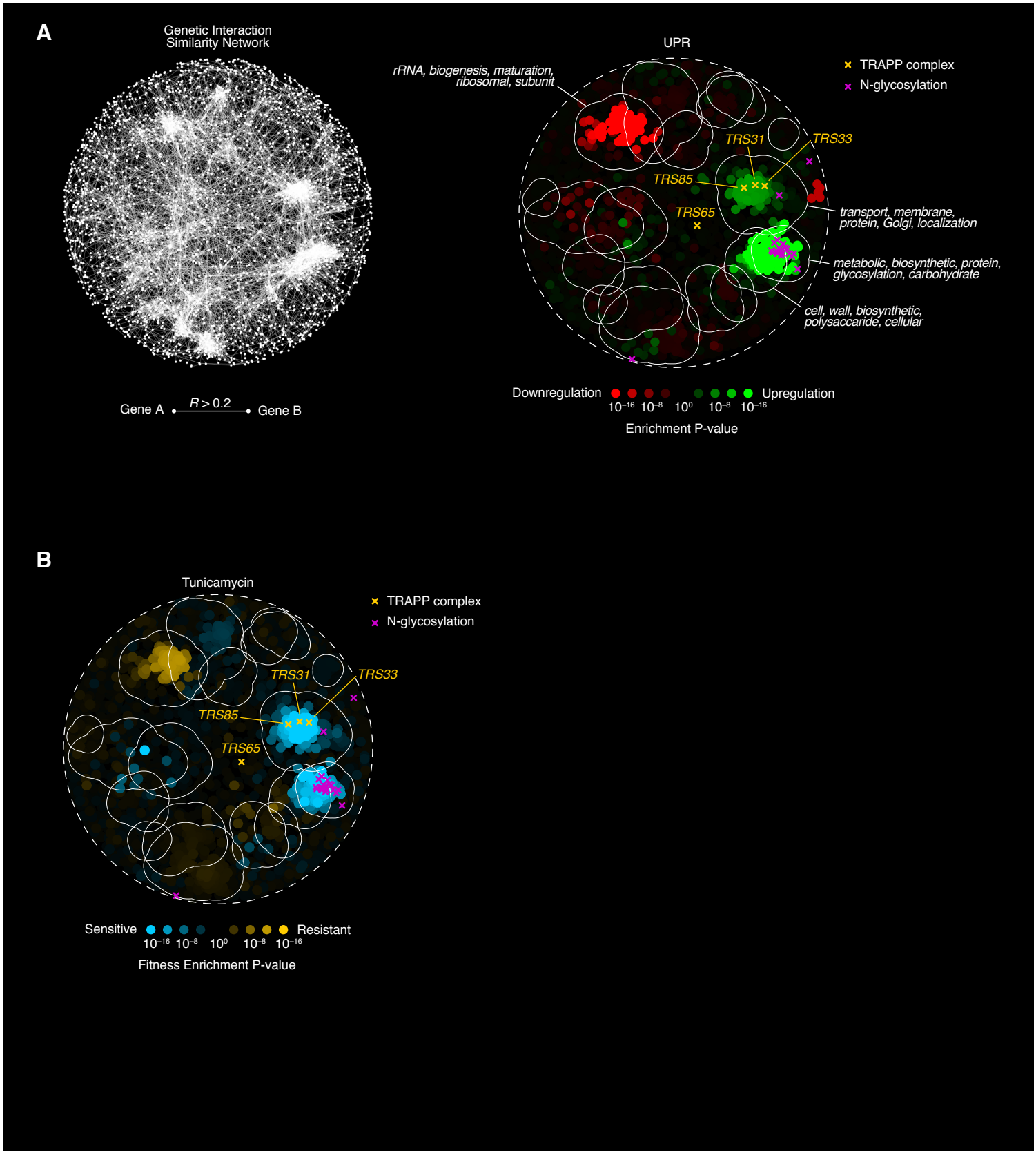

Supplemental Figure S5

A. 5 dpf, liver extracts

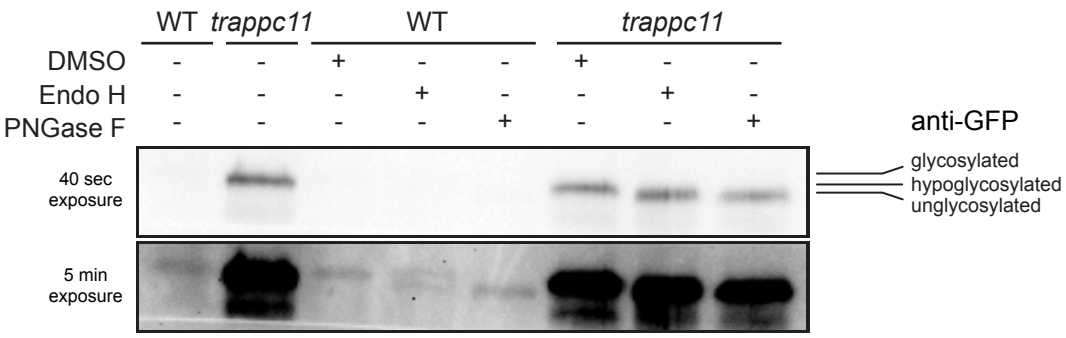

B.

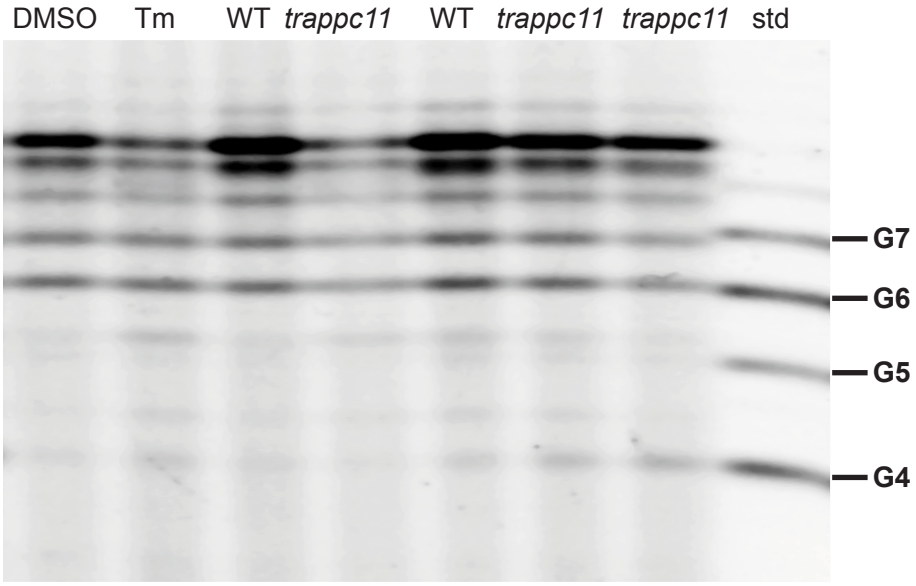

Supplemental Figure S6

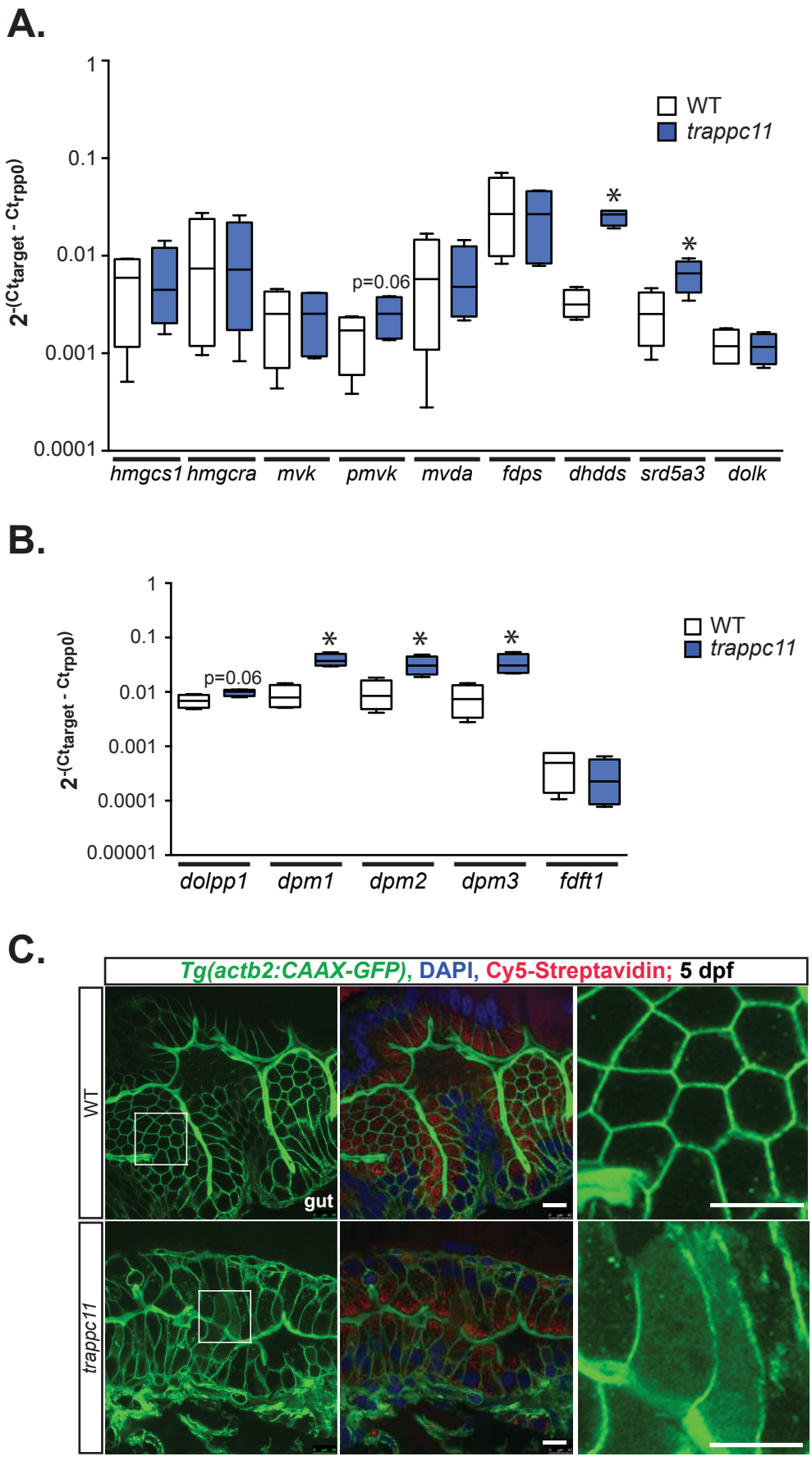

Supplemental Figure S7

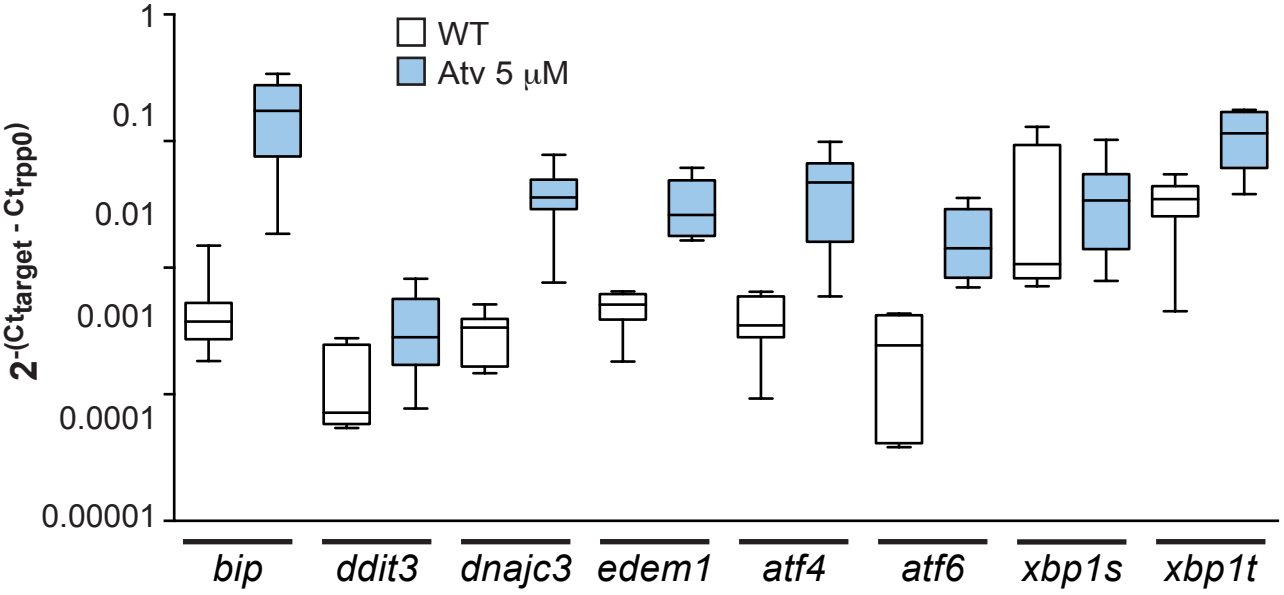

Supplemental Figure S8

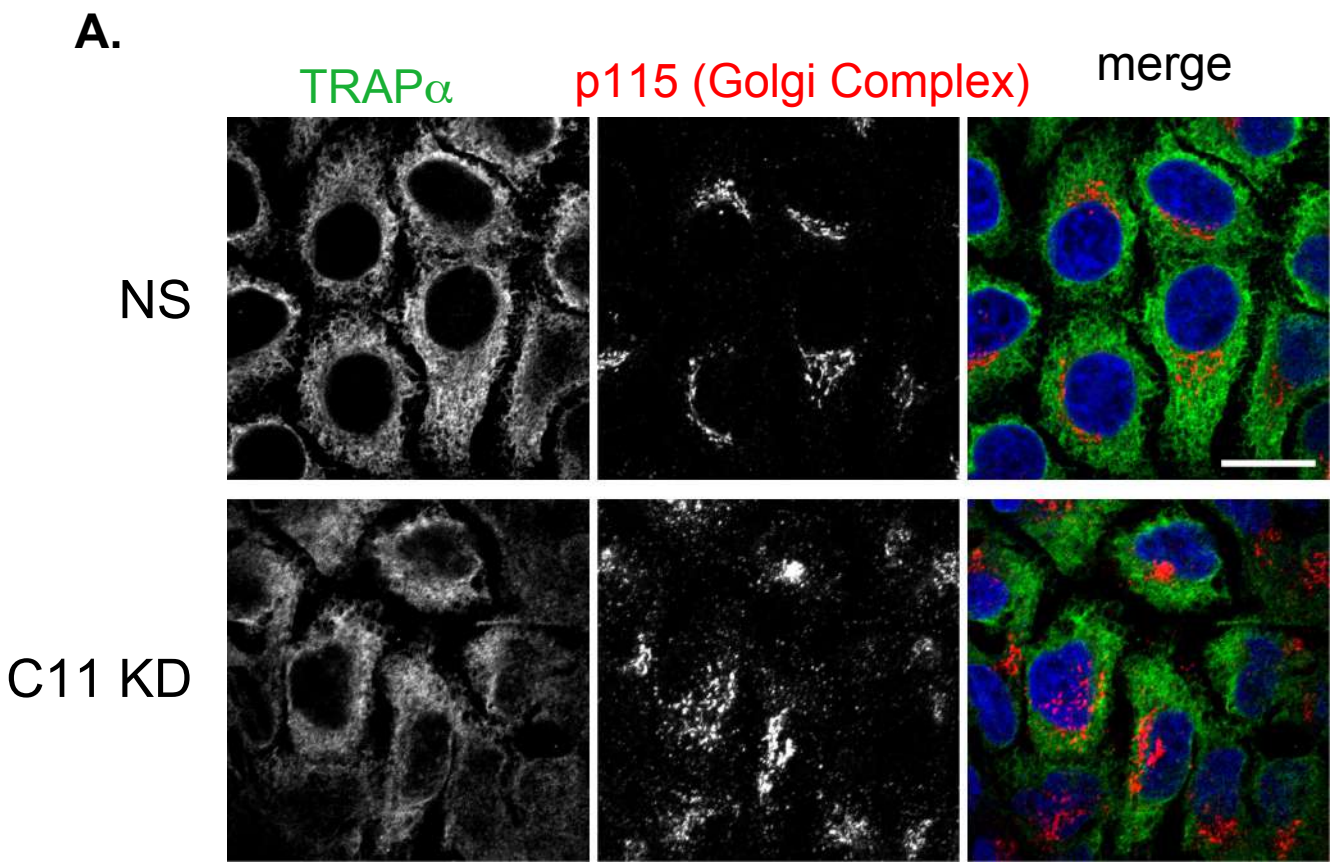

TABLE S1. Primer Sequences

Gene name	***Primer name/gene abbreviation***	**sequence – 5'-3'**
Asparagine-linked glycosylation 2 homolog	alg2-F	GTGTTCCTGCACCCTGATCT
	alg2-R	AGCACAGAGAGCGTGGAAAT
Asparagine-linked glycosylation 5 homolog	alg5-F	TCTAATGGCTGATGCTGACG
	alg5-R	ATCGCTGAGCCACTGATTCT
Asparagine-linked glycosylation 9 homolog	alg9-F	GTTCTGTGCTGCTGTTTGGA
	alg9-R	CCGACACAAACATTGACCAG
Activating transcription factor 4	atf4-F	TTAGCGATTGCTCCGATAGC
	atf4-R	GCTGCGGTTTTATTCTGCTC
Activating transcription factor 6	atf6-F	CTGTGGTGAAACCTCCACCT
	atf6-R	CATGGTGACCACAGGAGATG
Glucose-regulated protein, 78kD (also called bip)	bip-F	AAGAGGCCGAAGAGAAGGAC
	bip-R	AGCAGCAGAGCCTCGAAATA
DNA-damage-inducible transcript 3	ddit3-F	AAGGAAAGTGCAGGAGCTGA
	ddit3-R	TCACGCTCTCCACAAGAAGA
Dehydrodolichyl diphosphate synthase	dhdds-F	AAATGGCATGGGGAGTCGAG
	dhdds-R	CGAATACGAGGTCTGCCACA
DnaJ homolog, subfamily C, member	dnajc3-F	TCCCATGGATCCTGAGAGTC
	dnajc3-R	CTCCTGTGTGTGAGGGGTCT
Dolichol kinase	dolk-F	GAGAGAAACAGGTCTAACTGGCT
	dolk-R	TGGATCCATCTGCATGACTGC
Dolichyldiphosphatase 1	dolpp1-F	TCGCGATCCTTGTCGGATTC
	dolpp1-R	GACTGAACTGTGACCTCCGC
Dolichyl-phosphate N-acetylglucosaminephosphotransferase 1	dpagt1-F	CTCGGCCACTTTAGCAAGAC
	dpagt1-R	GTAGCTCATGCCCAGCTTTC
Dolichyl-phosphate mannosyltransferase polypeptide 1, catalytic subunit	dpm1-F	CACGGCATTAAACATGCAAC
	dpm1-R	GTTTGCCCCTCGACTGATAA
Dolichyl-phosphate mannosyltransferase polypeptide 2, regulatory subunit	dpm2-F	CACGTTCGTAATGGCAACCG
	dpm2-R	TCTCGTGGAAGAAAATAGCTGTG
Dolichyl-phosphate mannosyltransferase polypeptide 3	dpm3-F	GCTGGCATTGAATAGTAGGTGGA
	dpm3-R	TGGGGCAGCAAATGCAAATC
ER degradation enhancer, mannosidase alpha-like 1	edem1-F	ATCCAAAGAAGATCGCATGG
	edem1-R	TCTCTCCCTGAAACGCTGAT
Farnesyl-diphosphate farnesyltransferase 1	fdft1-F	TGAGGACCTGCTACGCCTAT
	fdft1-R	AGGAACGTGTGGAAGTCCTG
Farnesyl diphosphate synthase	fdps-F	AGCTAGAGGCATGTTACGGC
	fdps-R	AGCATGAGGCAGATTCTTAGCA
Glucosidase 1	gcs1-F	CGCAGCAAAGTACCATCTGA
	gcs1-R	AACCACTCGAACCAAACCTG
GDP-mannose pyrophosphorylase B	gmppb-F	CCCAAACCACTCGTTGAGTT
	gmppb-R	GCGGTTCCTAGAGGCTCTTT
3-hydroxy-3-methylglutaryl-Coenzyme A reductase a	hmgcra-F	CTGAGGCTCTGGTGGACGTG
	hmgcra-R	CGCCGCAGCTACGATGTTGGCG
3-hydroxy-3-methylglutaryl-Coenzyme A synthase 1	hmgcs1-F	CTCACTCGTGTGGACGAGAA
	hmgcs1-R	GATACGGGGCATCTTCTTGA
Mannose phosphate isomerase	mpi-F	AGAAGCCGCAGGTAAAGACA
	mpi-R	AACACGCCATACACTCCACA

Mevalonate (diphospho) decarboxylase a	mvda-F	CGAGCCACCTTCTGAAGTACA
	mvda-R	TAGGTGGGTAGGTGTCCAGG
Mevalonate kinase	mvk-F	CACACTTTTGCGACCAGAGA
	mvk-R	CAGCAGCAATGAGCATCTGT
Phosphomannomutase 2	pmm2-F	GCAGCCAACAGGAAAGAATC
	pmm2-R	CCAGCCTTCTGGAAACACAT
Phosphomevalonate kinase	pmvk-F	GCAGCCCGTCTGGATAATCA
	pmvk-R	TCGGACTCAGCGTCGTCTAT
Ribosomal protein/large/p0	rpp0-F	CTGAACATCTCGCCCTTCTC
	rpp0-R	TAGCCGATCTGCAGACACAC
DnaJ homolog, subfamily C, member	dnajc3-F	TCCCATGGATCCTGAGAGTC
	dnajc3-R	CTCCTGTGTGTGAGGGGTCT
Steroid 5 alpha-reductase 3	srd5a3-F	GGACTGACAGCTCAGGTAAAGT
	srd5a3-R	AACGTACAGCACCACCATCC
X box binding protein-1 (spliced; xbp1-s)	xbp1s-F	TGTTGCGAGACAAGACGA
	xbp1s-R	CCTGCACCTGCTGCGGACT
X box binding protein-1 (total; xbp1-t)	xbp1t-F	GAGGAGCCCACAAAGTCCTC
	xbp1t-R	CGAAGTGCTTTTTCCTCTGG